NASA Contractor Report 191150

Probabilistic Micromechanics for High-Temperature Composites

J.N. Reddy
Virginia Polytechnic Institute and State University
Blacksburg, Virginia

September 1993

Prepared for
Lewis Research Center
Under Contract NAG3–933

National Aeronautics and Space Administration

PROBABILISTIC MICROMECHANICS FOR HIGH–TEMPERATURE COMPOSITES

Grant Number: NAG–3–933; Period: Oct. 1, 1988–March 31, 1992

Principal Investigator: J. N. Reddy
Department of Engineering Science and Mechanics
Virginia Polytechnic Institute and State University
Blacksburg, Virginia 24061

RESEARCH OBJECTIVE

The three–year program of research had the following technical objectives: the development of probabilistic methods for micromechanics–based constitutive and failure models, application of the probabilistic methodology in the evaluation of various composite materials and simulation of expected uncertainties in unidirectional fiber composite properties, and influence of the uncertainties in composite properties on the structural response. The first year of research was devoted to the development of probabilistic methodology for micromechanics models. The second year of research focused on the evaluation of the Chamis–Hopkins constitutive model and Aboudi constitutive model using the methodology developed in the first year of research. The third year of research was devoted to the development of probabilistic finite element analysis procedures for laminated composite plate and shell structures.

TECHNICAL APPROACH AND RESEARCH ACCOMPLISHED

To simulate variations and uncertainties in constituent properties and manufacturing nonuniformities, as they would apply to high–temperature, metal–matrix composite materials and structures, the nonlinear behavior of the constituents was considered. The first phase of the research dealt with the linear micromechanics relations for metal–matrix composites using reference temperatures and zero load values.

The second phase involved the nonlinear characteristics (i.e. use of the power–law relations) and cyclic degradation effects. A Monte Carlo simulation routine has been built

around the METCAN program. The METCAN program (METal matrix Composite ANalyzer) uses the Chamis–Hopkins semi–empirical micromechanics equations in conjunction with a constituent based nonlinear power law to perform nonlinear analysis of fiber reinforced metal matrix composites. The research of the second phase was divided into three parts. The first part dealt with the linear studies, the second concerned with the nonlinear studies, and the third included comparisons between the Chamis–Hopkins micromechanics model and the Aboudi model.

The third phase of research involved application of the research performed in the first two phases to the analysis of laminated composite plates and shells. A 3–D degenerated shell element formulation, incorporating the first–order shear deformable kinematics, is used in conjunction with the first–order second moment technique for probabilistic analysis. Linear elastic composite behavior is modeled as well as nonlinear material behavior using the micromechanics theory of Aboudi and the classical rate–independent incremental plasticity, Random variables include: the ply stiffnesses, orientation angles, ply thicknesses, as well as the constituent micro properties such as the fiber and matrix stiffnesses and volume ratios. The probabilistic finite element model is used to quantify the variability and uncertainty in the response of composite shell structures. The computational procedure is then used to perform reliability analysis of composite shell structures.

SIGNIFICANCE OF THE RESEARCH

The probabilistic micromechanics approach and probabilistic finite element analysis computational procedures developed during this research are the first ones for laminated composite plates and shells. The procedures can be used in the analysis and design of high temperature, metal–matrix and ceramic composite materials and structures. The results of

this research play a crucial role in the establishment of increased performance and durability limits of high–temperature composite structures.

PERSONNEL

J. N. Reddy (Principal investigator)

R. A. Arenburg (Ph.D. student; completed Ph.D., Dec. 1988)

S. P. Engelstad (Ph.D. student; completed Ph.D., Dec. 1990)

Filis Kokkinos (Ph.D. student; continuing student)

TECHNICAL PUBLICATIONS

1. J. N. Reddy, and S. P. Engelstad, "Probabilistic Micromechanics for High-Temperature Composites," Progress Report submitted to NASA Lewis, June 1989.

2. S. P. Engelstad and J. N. Reddy, "Probabilistic Micromechanics for Metal Matrix Composites," Interim Research Report, June 1990.

3. R. T. Arenburg and J. N. Reddy, "Analysis of Metal-Matrix Composite Structures-I. Micromechanics Constitutive Theory," *Computers & Structures*, Vol. 40, No. 6, pp. 1357-1368, 1991.

4. R. T. Arenburg and J. N. Reddy, "Analysis of Metal-Matrix Composite Structures-II. Laminate Analysis," *Computers & Structures*, Vol. 40, No. 6, pp. 1369-1385, 1991.

5. S. P. Engelstad, J. N. Reddy and N. F. Knight, Jr., "Postbuckling Response and Failure Prediction of Flat Rectangular Graphite-Epoxy Plates Loaded in Compression," *AIAA J.*, to appear.

6. S. P. Engelstad and J. N. Reddy, "Probabilistic Nonlinear Finite Element Analysis of Composite Structures," (with S. P. Engelstad), *AIAA J.*, to appear.

7. R. T. Arenburg and J. N. Reddy, "Applications of the Aboudi Micromechanics Theory to Metal Matrix Composites," *The Third-Joint ASCE/ASME Mechanics Conference*, July 9-12, 1989, University of California, San Diego, CA; paper appeared in: *Mechanics of Composite Materials and Structures*, J. N. Reddy and J. L. Teply (eds.), AMD-Vol. 100, pp. 33-40, The American Society of Mechanical Engineers, New York, 1989.

8. S. P. Engelstad and J. N. Reddy, "Probabilistic Micromechanics for Metal-Matrix Composites," *The Third-Joint ASCE/ASME Mechanics Conference*, July 9-12, 1989, University of California, San Diego, CA.

10. S. P. Engelstad and J. N. Reddy, "Nonlinear Probabilistic FEM for Composite Shells," *ASCE Engineering Mechanics Specialty Conference*, May 19-22, 1991, Columbus, OH.

11. S. P. Engelstad, J. N. Reddy, and D. A. Hopkins, "Probabilistic Micromechanics for Metal Matrix Composites," *1991 ASME Applied Mechanics and Biomechanics Summer Conference*, June 17-19, 1991, Columbus, Ohio; appeared in *Mechanics of Composites at Elevated and Cryogenic Temperatures*, S. N. Singhal, W. F. Jones, and C. T. Herakovich (eds.), AMD-Vol. 118, The American Society of Mechanical Engineers, New York, 1991, pp. 181-193.

12. S. P. Engelstad and J. N. Reddy, "Nonlinear Probabilistic Finite Element Modeling of Composite Shells," *First U.S. National Congress on Computational Mechanics*, Chicago, IL, July 21-24, 1991.

13. S. P. Engelstad and J. N. Reddy, "A Probabilistic Postbuckling Analysis of Composite Shells," *First Int. Conf. on Computational Stochastic Mechanics*, Corfu, Greece, Sept. 17-19, 1991; *Computational Stochastic Mechanics*, P. D. Spanos and C. A. Brebbia

(eds.), Computational Mechanics Publications and Elsevier Applied Science, pp. 839-850, 1991.

14. S. P. Engelstad, R. T. Arenburg, and J. N. Reddy, "Computational Models of Inelasticity in Composite Laminates," *COMPLAS III: Third Int. Conf. on Computational Plasticity Fundamentals and Applications*, Barcelona, Spain, April 6-10, 1992.

15. S. P. Engelstad, S. K. Jain and J. N. Reddy, "On the Application of Incremental Theory of Plasticity with Endochronic Hardening Rule," *COMPLAS III: Third Int. Conf. on Computational Plasticity Fundamentals and Applications*, Barcelona, Spain, April 6-10, 1992.

16. S. P. Engelstad and J. N. Reddy, "Nonlinear Probabilistic Finite Element Models of Laminated Composite Shells," (with S. P. Engelstad), Research Report No. CCMS-91-02, Virginia Polytechnic Institute and State University, Blacksburg, Virginia, Jan. 1991.

TECHNICAL DISCUSSION

1. Introduction

The current emphasis for computational analysis of high temperature metal matrix composites involves micromechanics theories with nonlinear behavior occurring at the constituent level. Interphase regions are included in these models, as studies have shown that residual stresses that occur in the composites can be controlled by appropriate choice of an interphase material and thickness. Both ply and constituent level failure theories are employed in the resultant schemes. The procedures, due to the use of constituent level material properties as the primitive variables, can be used to predict the qualitative behavior of new composites prior to any experimental measurements. Material properties, strengths, and stress–strain data are useful predictions. However, since uncertainties are present in the constituent properties, volume ratios, and fabrication variables, the results lack the variability that is always present in experimental data (see [1–4]).

A previous study by Stock [4] proposed that constituent level uncertainties be modeled using statistical distributions and the resultant composite micromechanics models and laminate theories be used to predict the statistical scatter in experimentally observed composite properties. A computer code developed at NASA Lewis, called ICAN (Integrated Composite Analyzer), for comprehensive linear analysis of multilevel fiber composite structures was the deterministic basis of the simulation model. Monte Carlo simulation methods were used to model the probabilistic distributions in the primitive variables, and distribution results for material properties and strengths of a graphite–epoxy ply were presented. The probabilistic micromechanics model proved quite useful in predicting the experimental scatter of these linear composite structures.

Advanced composites such as the metal matrix composites are used in aerospace structures where operating temperatures exceed the limits of organic matrix composites. Therefore, researchers have focused on the development of suitable constitutive theories for these materials. Dvorak and Bahei–El–Din [5–9] introduced a computationally simple

micromechanics model based on what they refer to as a "vanishing fiber diameter model". The model has been used in the analysis of a variety of laminated composites [10–12].

The power–law model of Hopkins and Chamis [1] is based on the assumption of strain compatibility and stress equilibrium. In this model the representative volume element is subdivided into several distinct phases. The different phases are used to represent the fiber, an interphase region and three matrix subregions. The matrix subregions were introduced to characterize the through–the–thickness variation of the matrix phase.

The "periodic hexagonal array" (PHA) model of Teply and Dvorak [13,14] is developed by considering a hexagonal fiber array as the representative cell. This leads to the use of a triangular representative volume element which is analyzed utilizing the finite element method. Both displacement and equilibrium formulations are examined to establish upper and lower bounds on the instantaneous properties of the composite.

Aboudi [15–20] developed a comprehensive micromechanics theory which has its origins in the work of Achenbach and his colleagues [21,22]. The theory is applicable to several types of composites, such as particulate, short–fiber or continuous–fiber reinforcement. Unlike most micromechanics theories, the Aboudi theory is not restricted to the assumption of perfect fiber/matrix bonding. Instead, an infinitely thin elastic interface is assumed which allows the simulation of fiber/matrix damage or an interphase region. The Aboudi micromechanics theory can be viewed as a variational formulation of the displacement or stress boundary value problem at the micromechanics level (see [23–25]).

Another approach taken by many researchers when modeling metal matrix composites does not involve micromechanics level analysis. They attempt to model the material nonlinearity using macroscopic yield criteria to account for the anisotropic behavior. Many authors have made contributions in this area; however, only a few are discussed here for brevity. Hill's anisotropic theory of plasticity [26] has received much

attention. This theory was based on a generation of the von mises yield criterion which assumed yielding was independent of hydrostatic stress and that plastic flow was incompressible. Whereas these assumptions are standard and experimentally validated for metals, they have been shown to be incorrect for some composite materials. A recent yield function was introduced by Sun et al. [27,28], which was selected for this work. The function is quadratic in stresses and, in general, excludes the assumptions of incompressibility of plastic strains and that no yielding is caused by hydrostatic stresses.

It is the objective of this study to quantify the variability present in metal matrix composites. In the first model, the probabilistic micromechanics concept developed by Stock [4] to apply to the nonlinear constitutive behavior of high temperature metal matrix composites. The Monte Carlo procedure is employed in conjunction with the METCAN program (METal matrix Composite ANalyzer) developed at NASA Lewis Research Center. Assumed statistical distributions for material properties, volume ratios, and nonlinear parameters thus allow prediction of experimental scatter in metal matrix composite behavior. In the second model, a macromechanics (orthotropic) elastoplasticity theory is combined with a continuum shell element (see Reddy and his colleagues [29,30]) and a probabilistic methodology is incorporated to account for uncertainties in material properties. The resulting formulation is used to quantify the variability of the structural response of materially nonlinear composite laminates. Numerical examples based on the formulation are also discussed here.

2. Micromechanics Constitutive Model

2.1 Micromechanics Formulation

The deterministic part of the model consists of the computational scheme contained in the METCAN program. It employs the Chamis–Hopkins semi–empirical micromechanics equations [1] in conjunction with a constituent based multi–factor nonlinear material model [2,3] to perform nonlinear analysis of fiber reinforced metal

matrix composites. As shown in Fig. 1, a closed–loop analysis logic is used in which nonlinearities are applied at the micromechanics (constituent) level, ply properties are constructed in the synthesis stage, laminate theory is used to build laminate properties, global analysis is performed, and the laminate is decomposed again to the constituent level. Note that the Monte Carlo sampling is performed at the constituent level. In the decomposition stage, the ply stresses are computed and used to calculate the stresses in the constituents (microstresses). The constituent material properties are updated based on their dependency on various factors in the nonlinear material model including stress, temperature, time, mechanical and thermal cycles. The resultant nonlinear analysis involves incremental loading and time stepping in which iterative convergence is checked at the micro, ply and laminate scales.

The multi–factor material model is presented in Figure 2 along with the representative subcell of the micromechanics relations. This material model has been selected to consistently represent the in–situ behavior of all constituent properties. More details on this model can be found in the work by Hopkins [2]. The unit cell presented in Figure 2 illustrates the various subregions assumed in the micromechanics theory to capture the effects of matrix, interphase, and fiber interaction.

2.2 Monte Carlo Simulation

Monte Carlo simulation is a computational technique often used to simulate random processes. In a general sense, it is defined as any computer simulation involving random numbers for solving stochastic problems. In the procedure, the computer is used to generate independent statistical samples for each random variable, which are then fed into the model. Each sample can be thought of as an independent deterministic experiment, which is processed by the model to yield the results of the experiment. Each sample is drawn from an appropriate probability distribution. Following the simulation process, the output data is statistically analyzed to estimate the true characteristics of the model. The

law of large numbers assures that if sufficiently large sample sizes are taken, the results will converge to the true population statistics of the model.

3. Macromechanics Constitutive/Structural Model

3.1 Orthotropic Plasticity Formulation

In order to model orthotropic elastoplastic behavior from a macroscopic viewpoint, a quadratic yield function introduced by Sun, et al. [27,28] is adopted. The yield function is quadratic in the stresses and employs the associative flow rule and isotropic hardening. The plane stress radial return algorithm of Simo and his colleagues [31,32] was modified to include this new yield function. This algorithm was chosen due to its accuracy, improved global convergence rates, and compatibility with the probabilistic finite element routines.

Governing Equations

According to Sun [27], the orthotropic yield function is given by

$$f = \frac{1}{2}(a_{11}\sigma_{11}^2 + a_{22}\sigma_{22}^2 + a_{33}\sigma_{33}^2 + 2a_{12}\sigma_{11}\sigma_{22} + 2a_{13}\sigma_{11}\sigma_{33}$$

$$+ 2a_{23}\sigma_{22}\sigma_{33} + 2a_{44}\sigma_{23}^2 + 2a_{55}\sigma_{13}^2 + 2a_{66}\sigma_{12}^2) = \bar{Y} \qquad (1)$$

where $\bar{Y}$ is a state variable and σ_{ij} are the stresses in principal material coordinates. The coefficients a_{ij} are constants, which are determined from experimental data and control the amount of anisotropy in the plastic behavior. This yield criterion does not include the assumption of incompressibility of plastic strains or that hydrostatic stresses result in no yielding or plastic deformation. The function also reduces to the von Mises criterion or the Hill yield function for orthotropic materials [26] with appropriate selection of the a_{ij} values.

The associative flow rule assumption allows the incremental plastic strains to be stated as

$$d\epsilon^{P}_{ij} = d\gamma \frac{\partial f}{\partial \sigma_{ij}} \tag{2}$$

The shell finite element employed is a continuum element developed from the 3–D elasticity theory using the kinematics of the first order shear deformation theory (see [29,30]). In other words, transverse normals remain straight and inextensible, so that $\epsilon_{33} = 0$. Consequently, σ_{33} does not enter the formulation (because the strain energy of the shell due to ϵ_{33} is zero).

In vector notation, the stress and strain tensors can be written as

$$\{\sigma\} = \{\sigma_{11}\ \sigma_{22}\ \sigma_{12}\ \sigma_{13}\ \sigma_{23}\}^{T}$$

$$\{\epsilon\} = \{\epsilon_{11}\ \epsilon_{22}\ 2\epsilon_{12}\ 2\epsilon_{13}\ 2\epsilon_{23}\}^{T}\ ,\ \{\epsilon^{P}\} = \{\epsilon^{P}_{11}\ \epsilon^{P}_{22}\ 2\epsilon^{P}_{12}\ 2\epsilon^{P}_{13}\ 2\epsilon^{P}_{23}\}^{T} \tag{3}$$

The components of the back stress q_{ij} (included to model kinematic hardening), and the relative stress $\eta_{ij} = \sigma_{ij} - q_{ij}$ are expressed in the vector form as

$$\{q\} = \{q_{11}\ q_{22}\ q_{12}\ q_{13}\ q_{23}\}^{T}\ ,\ \{\eta\} = \{\eta_{11}\ \eta_{22}\ \eta_{12}\ \eta_{13}\ \eta_{23}\}^{T} \tag{4}$$

Thus the governing elastoplastic equations in vector form can be expressed as (see [31])

$$\{\epsilon\} = \{\epsilon^{e}\} + \{\epsilon^{P}\}$$

$$\{\sigma\} = [Q]\{\epsilon^{e}\}$$

$$\{\dot{\epsilon}^{P}\} = \dot{\gamma}[P]\{\eta\}$$

$$\{\dot{q}\} = \dot{\gamma}\frac{2}{3}H'[P]\{\eta\}$$

$$f = \frac{1}{2}\{\eta\}^T[P]\{\eta\} - \frac{1}{3}Y^2(\alpha) \leq 0$$
$$\dot{\alpha} = \dot{\gamma}\left[\frac{2}{3}\{\eta\}^T[P]\{\eta\}\right]^{1/2} \tag{5}$$

where $\dot{\gamma}$ is the time derivative of the plastic load parameter, H' is the kinematic hardening modulus, and the parameter Y represents the hardening law in terms of the equivalent plastic strain α. The matrix [Q] is the elastic constitutive matrix, adjusted for the constraint $\sigma_{33} = 0$. The effective stress $\bar{\sigma}$ can be expressed as

$$\bar{\sigma} = \sqrt{\frac{3}{2}\{\eta\}^T[P]\{\eta\}} \tag{6}$$

and matrix [P] is given by

$$[P] = \begin{bmatrix} a_{11} & a_{12} & 0 & 0 & 0 \\ a_{12} & a_{22} & 0 & 0 & 0 \\ 0 & 0 & 2a_{66} & 0 & 0 \\ 0 & 0 & 0 & 2a_{55} & 0 \\ 0 & 0 & 0 & 0 & 2a_{44} \end{bmatrix}. \tag{7}$$

Loading and unloading conditions are stated in the Kuhn–Tucker form [32] by requiring that

$$f \leq 0\ ,\ \dot{\gamma} \geq 0\ ,\ \dot{\gamma} f \equiv 0 \tag{8}$$

For an elastic process, $f < 0$ and $\gamma = 0$. For a plastic process, we have $f = 0$ and $\gamma > 0$. These two conditions are generally valid, for a loading or unloading state.

Incremental Formulation

The ordinary differential equations of time in Eq. (5) can be numerically integrated using a backward Euler difference scheme over the time interval (t_n, t_{n+1}). Letting $\gamma_{n+1} = \dot{\gamma}_{n+1}\Delta t$ (the plastic load parameter) and $\bar{f} = \sqrt{\{\eta\}^T[P]\{\eta\}}$, the strain at t_{n+1} can be

written in terms of the strain at t_n and the gradient of the incremental displacements,

$$\{\epsilon_{n+1}\} = \{\epsilon_n\} + \nabla\{\Delta u\} \tag{9}$$

where "∇" denotes the differential operator used in the definition of strains. A trial stress state is assumed by freezing plastic flow so that the entire step is purely elastic. The trial stress then becomes

$$\{\sigma^{trial}_{n+1}\} = [Q](\{\epsilon_{n+1}\} - \{\epsilon^P_n\})$$

$$\{\eta^{trial}_{n+1}\} = \{\sigma^{trial}_{n+1}\} - \{q_n\}$$

$$\{\epsilon^P_{n+1}\} = \{\epsilon^P_n\} + \gamma_{n+1}[P]\{\eta_{n+1}\}$$

$$\{q_{n+1}\} = \{q_n\} + \gamma_{n+1}\frac{2}{3}H'[P]\{\eta_{n+1}\}$$

$$\alpha_{n+1} = \alpha_n + \sqrt{\frac{2}{3}}\,\gamma_{n+1}\bar{f}_{n+1}. \tag{10}$$

In order to perform the incremental updates required in equations (10), the plastic load parameter (Lagrange multiplier) γ must be determined. It is found by enforcing the consistency condition at time t_{n+1}, i.e.,

$$f^2(\gamma_{n+1}) \equiv \frac{1}{2}\bar{f}^2_{n+1} - \frac{1}{3}[Y(\alpha_n + \sqrt{\frac{2}{3}}\,\gamma_{n+1}\bar{f}_{n+1})]^2 = 0. \tag{11}$$

The actual hardening functions used in the program are those recommended by Simo and Hughes [31],

$$Y(\alpha) = \beta\bar{H}\alpha + \sigma_Y + (K_\infty - \sigma_Y)[1 - \exp(-\lambda\alpha)] \tag{12}$$

and by Sun [27],

$$Y(\alpha) = \bar{H}\left[\alpha + \left[\frac{\sigma_Y}{\bar{H}}\right]^{\lambda}\right]^{1/\lambda}, \tag{13}$$

where $\bar{H}$ is the hardening modulus, σ_Y the uniaxial yield stress, K_∞ and λ are other input parameters, and

$$H(\alpha) = (1-\beta)\bar{H}\alpha.$$

Here β denotes the fraction of kinematic and isotropic hardening desired, i.e. $\beta = 1$ denotes purely isotropic hardening, and $\beta = 0$ denotes purely kinematic hardening. Equation (11) is solved at each gauss point in the structure for γ by a local Newton iteration procedure, as it is generally a nonlinear scalar equation.

The global equilibrium is obtained by using Newton–Raphson iteration. This requires that the tangent moduli be known in the form

$$[Q^{eP}]_{n+1} = \left\{\frac{d\sigma}{d\epsilon}\right\}_{n+1} \tag{14}$$

Simo and Hughes [31] developed tangent moduli, which are consistent with the integration algorithm previously discussed. For finite values of load step size, they showed that the consistent elastoplastic tangent moduli preserved the quadratic rate of asymptotic convergence that is characteristic of Newton's method. Use of the continuum tangent moduli derived independent of the algorithm loses this convergence rate.

3.2 Continuum–Based Finite Element

The incremental equations of a continuous medium are formulated based on the principle of virtual displacements and the total Lagrangian description. The detailed description can be found in [29,30]. The final incremental equilibrium equations for an element are given by

$$([K_L] + [K_{NL}])\{\Delta\} = \{R\} - \{F\} \tag{15a}$$

where $\{\Delta\}$ is the vector of nodal incremental displacements in an element, and $[K_L]$, $[K_{NL}]$, and $\{F\}$ are defined by,

$$[K_L] = \int_V [B_L]^T [Q][B_L] dV$$

$$[K_{NL}] = \int_V [B_{NL}][Q][B_{NL}] dV$$

$$\{F\} = \int_V [B_L]\{\hat{S}\} dV. \tag{15b}$$

In the above equations, $[B_L]$ and $[B_{NL}]$ are linear and nonlinear strain–displacement transformation matrices, $[Q]$ is the incremental stress–strain material property matrix, $\{\hat{S}\}$ is a vector of 2nd–Piola–Kirchhoff stresses, and $\{R\}$ is the external load vector. All matrix elements refer to the deformed state with respect to the original undeformed configuration.

After assembly, the following linearized versions of the actual equilibrium equations are obtained

$$[\hat{K}]\{\Delta\} = \{\hat{R}\}, \tag{16}$$

where

$$[\hat{K}] = [K_L] + [K_{NL}]$$
$$[\hat{R}] = \{R\} - \{F\} \tag{17}$$

The Newton–Raphson method is employed to solve the linearized equations iteratively until the actual equations of motion are satisfied to a required tolerance.

In the process of evaluating the integrals in equation (15), Gauss quadrature is used in the membrane directions of the shell, and in the thickness direction when plasticity occurs. When material behavior is elastic at a membrane location through the entire laminate thickness, then explicit integration is performed in the thickness direction.

3.3 Second–Moment Formulation

The second–moment perturbation method as developed by Liu, et al. [33,34] is summarized in this section for geometric and material nonlinear time independent behavior.

The equilibrium equation for the probabilistic finite element model can be expressed as

$$\{F(\{\Delta\},\{b\})\} = \{R(\{b\})\} \tag{18}$$

where $\{F\}$ is the internal force vector, $\{\Delta\}$ is the displacement vector, $\{R\}$ is the external force, and $\{b\}$ is a discretized vector of the random function $b(\underline{x})$, where $\underline{x}$ is a spatial coordinate $\{\underline{x}\}$. The random function $b(\underline{x})$ is expanded using shape functions $\psi_i(\underline{x})$:

$$b(\underline{x}) = \sum_{i=1}^{n} \psi_i(\underline{x}) b_i \tag{19}$$

where b_i are the nodal values of $b(\underline{x})$. Generally the random quantity b can be a material property, geometric dimension, or a load.

The probabilistic finite element analysis is carried out by applying the second–moment method. The vectors in equation (18) are expanded about the mean of the random function b via Taylor's series, and the following perturbation equations are obtained:

Zeroth–order equation:

$$\{\bar{F}\} = \{\bar{R}\} \tag{20}$$

First–order equations:

$$[\bar{K}^T]\{\bar{\Delta}\}_{b_i} = \{\bar{R}\}_{b_i} - \{\bar{F}\}_{b_i} \ , \ i = 1,...,n \tag{21}$$

where the bar over the symbols represent evaluation of that term at the mean value of b, and the subscript b_i represents the derivative with respect to b_i. Also $[K^T]$ is defined to be the tangent stiffness matrix,

$$[K^T] = \frac{\{\partial F\}}{\{\partial \Delta\}} \tag{22}$$

Once $\{\bar{\Delta}\}$ and $\{\bar{\Delta}\}_{b_i}$ are obtained by solving equations (20) and (21), the mean and autocovariance matrices for the nodal displacements can be determined (see [38]).

The solution procedure involves a consecutive solution of equations (20) and (21). After the deterministic zeroth–order equation (21) is solved, either once for the linear case or iteratively at each load step in the nonlinear case, the generalized displacement vector $\{\bar{\Delta}\}$ is used to perform the perturbation solutions in equation (21). In (21), there are as many solutions for $\{\Delta\}_{b_i}$ as there are number of nodes in the model. In addition, the computations must be performed for each layer in the model, as a particular random function is assumed to be independent from layer to layer. If there are n nodes and P layers in the model, (n + 1)P more matrix solutions are required at each load step for each random variable. This is not as expensive as it seems, because the stiffness matrix $[\bar{K}^T]$ is inverted once and used in (21).

For materially nonlinear problems the residual vector can be functionally represented in the form

$$\{F\} = \{F(\{\Delta\},\{b\})\} \tag{23}$$

Temporarily dropping the vector braces, and differentiating F with respect to b, we obtain

$$\frac{dF}{db} = \frac{\partial F}{\partial b} + \frac{\partial F}{\partial \Delta}\frac{\partial \Delta}{\partial b} \tag{24}$$

The first term on the right hand side involves the explicit derivative of F with respect to b. This is the derivative that must be evaluated on the right side of equation (21). This derivative can be expressed exactly when elastic behavior exists. However, when material nonlinear behavior is present, finite difference derivatives are used (as in [33]) once again due to the complex nonlinear relationship between stress and strain. Since orthotropic plasticity is present in certain layers, the radial return algorithm discussed previously is considered to be very good for this purpose (see [33]). This is true since at a particular load step, the plastic strain and effective plastic strain are "frozen" and only updated after equilibrium conversion is achieved. This update can be done after the finite difference calculations are made, so that the true effect of perturbing the random variable about its mean is measured. Other advantages of the radial return method are the increased accuracy involved in the stress recovery routine and the algorithmic compatible tangent moduli which results in a more accurate tangent stiffness matrix. This accuracy is important in computing the perturbation derivatives [e.g., $\{\bar{\Delta}\}_{b_i}$ in equation (21)].

Sources of randomness in the model can be material properties, geometric dimensions, or loads. In the present study, the ply thickness, ply angle and material properties are selected as the random variables. The random material variables include the engineering properties $E_{11}, E_{22}, \nu_{12}, G_{12}, G_{13}, G_{23}$, and the plasticity parameters σ_y and $\bar{H}$ (uniaxial yield stress and hardening modulus). The loading is considered to be deterministic throughout this study. For details regarding the incorporation of these variables, see Reference 38.

The probabilistic finite element procedure developed herein has the ability to model the spatial correlation involved in random fields. This technique is discussed in detail in [38], where examples involving random fields were included. However in the present work

it is assumed that fully correlated fields exist in each ply which degenerate to single random variables, and each random variable is independent from ply to ply.

4. Applications

4.1 Micromechanics Constitutive Model

Linear Analysis

First, simulations were performed in which the nonlinear multi–factor material model was not activated. As in Stock's work [4] histograms, cumulative distribution, and confidence interval curves were used as methods of illustrating various characteristics of a single ply. P100 high modulus graphite fiber and a copper matrix were selected as the constituents for this linear work. In general, sample sizes of 50 were chosen as statistically significant to show the trends of interest and remain economical.

Histograms and cumulative distribution plots were made for the two cases given in Table 1. Case 1 represents a narrow range distribution of the constituent properties, and Case 2 a wide one. A deterministic case was run using the mean values from Cases 1 and 2 (given by either μ or β). Sample results are given in Figures 3a–d for the in–plane shear modulus $G_{\ell 12}$ results. These are compared to the deterministic case result of 32.2 GPa to assess the sensitivity of the ply properties to changes in the distribution parameters.

Confidence interval curves are used to investigate and illustrate various effects on the resultant ply properties. These effects include fiber and matrix strengths, fiber orientation, fiber stiffnesses, and interphase thickness. Some examples of these effects are presented next.

Fiber Strength Effect. Using the properties of Case 1 as the base, the shape parameter of the Weibull distribution for fiber strength was perturbed to show the effects on the ply properties. The fiber volume ratio was kept deterministic and the simulation was performed for a range of these values. Figure 4 contains representative results for the ply longitudinal tensile strength. The solid lines represent the means of the samples, and

the stars above and below represent the upper and lower bounds of the 95% confidence interval estimates.

Matrix Strength Effect. Similar variations are made on the matrix strength shape parameters with the intent of showing the effects of these changes on ply strengths. These results are given in Figures 5 through 7.

Fiber Orientation Effect. Three values of the distribution parameter on fiber angle were simulated to determine the effect on the ply properties. These curves are given in Figures 8 through 11.

In general, from reviewing the previous confidence interval plots, the metal matrix composite ply properties are not very sensitive to fiber misalignment due to the closeness of the matrix modulus to the fiber modulus. It is also easy to see that ply longitudinal tensile strength is significantly affected by the shape parameter of fiber strength. Without further detail, it is evident that much information concerning the variability of this metal matrix composite has been quantified. The next step is to determine effects of allowing the nonlinear material model to become active.

Nonlinear Analysis

For any given particular ply property, the governing equation is the micromechanics relation shown in Fig. 2. This equation relates the ply property to the constituent properties, i.e., the fiber, matrix, and interphase properties. These constituent properties are in turn governed by the nonlinear multi–factor material model (power law), thereby making them a function of the local temperatures, stresses, stress rates, and mechanical and thermal cycles (see Figure 2). The constituent power laws contain certain allowable parameters such as melting temperature, strengths, allowable stress rates and cyclic thermal and mechanical strengths. In addition, the individual terms in the power law are raised to an exponent or power.

In this section, in addition to the random variables used in the linear analyses, the allowable parameters in the power law terms and the exponents were included as random variables. The material studied is Silicon Carbide fiber (SCS–6) in a Titanium Aluminide matrix (TI15). Table 2 contains information on the distribution parameters for each random variable. For illustrative purposes, confidence interval plots are used again to investigate the effects on the ply longitudinal tensile strength. The fiber volume ratio is deterministic and a sample size of 50 is again chosen.

Longitudinal Tensile Strength. The micromechanics equation for longitudinal tensile strength is given below for ease of discussion:

$$S_{\ell 11t} = S_{f11t}\left\{K_m\left[\frac{E_{m11}}{E_{f11}}\right] + \gamma K_f\left[\left[\frac{D}{D_o}\right]^2 + \left[1 - \left[\frac{D}{D_o}\right]^2\right]\frac{E_{d11}}{E_{f11}}\right]\right\} \tag{25}$$

The symbols K, γ and D indicate volume ratio, an empirical constant, and fiber diameter respectively. The nonlinear power law relationship for the appropriate constituent properties are,

$$S_{f11t} = S_{f11to}\left[\frac{T_{Mf} - T}{T_{Mf} - T_o}\right]^n\left[\frac{S_f - \tau}{S_f - \tau_o}\right]^m\left[\frac{\dot{S}_f - \dot{\tau}_o}{\dot{S}_f - \dot{\tau}}\right]^\ell\left[\frac{N_{MF} - N}{N_{MF} - N_o}\right]^q \tag{26}$$

$$E_{m11} = E_{m11o}\left[\frac{T_{Mm} - T}{T_{Mm} - T_o}\right]^n\left[\frac{S_m - \tau}{S_m - \tau_o}\right]^m\left[\frac{\dot{S}_m - \dot{\tau}_o}{\dot{S}_m - \dot{\tau}}\right]^\ell\left[\frac{N_{MF} - N}{N_{MF} - N_o}\right]^q \tag{27}$$

Similar relations hold for E_{d11} and E_{f11}. In order to have a basis for comparison, Figure 12, which contains no nonlinear effects, is included.

First the effects of the constituent property S_{f11t} are investigated. In Figures 13 and 14, the nonlinear temperature term is activated by elevating the ply to 811°K temperature.

Here the coefficient of variation (COV) of the temperature exponent n was varied from 1% to 30%, and the COV of the fiber melting temperature was varied from 1% to 10%. One can see that generally the S_{f11t} values were reduced when compared to the linear curve; however, little difference occurred for the perturbation on the melting temperature or the exponent n. As for the stress nonlinear power term, the Weibull distribution parameter for S_{f11t} was varied between 20 and 10 (narrow and wide) when a ply uniaxial stress of 68.9 MPa existed (see Figure 15). In order for the fiber tensile strength to behave linearly to stress changes as expected, the exponent m in the micromechanics equation was chosen to be zero (see Fig. 2). Thus the differences in the two curves shown in Figure 15 are simply due to the influence of the micromechanics equation and not the power law equation.

Next, the nonlinear behavior of the constituent E_{m11} was studied. Figure 16 shows the effect of simply varying the COV of E_{m11} without the power law terms being activated. One can see that the effects of changing E_{m11}'s distribution parameters are small. Figures 17 and 18 contain the results of activating the temperature term and perturbing the exponent n and the matrix melting temperature COV's in equation (27). Little changes due to the perturbed quantities are noticed for these results.

Figure 19 is an example of activating the mechanical cycle nonlinear power term. In this plot the Weibull distribution parameter for the mechanical cyclic strength N_{MF} was varied from 20 to 10. In this example, 5 x 10^5 cycles (50% of the assumed strength) was used. From this result, it can be concluded that the probabilistic distribution of cyclic strength is significant for this high degree of nonlinearity, as would be expected.

Obviously, the possibilities for analytical examples and investigations are voluminous. The previous examples are meant only to be representative of the capability. In addition, as in Stock [4], the individual ply could be broken down into subplies and the simulation procedure performed at this scale. Laminate theory can be used to build the ply properties, and in this way uncertainties caused by many fibers per layer or variations through the thickness is effectively modeled.

4.2 Macromechanics Constitutive/Structural Model

ARALL Laminate Tension Specimen with Hole

ARALL laminates are high strength hybrid composites developed by Alcoa for aerospace applications. Figure 20 illustrates the architecture of the laminate, which consists of thin sheets of high strength aluminum alloys bonded to high strength aramid fibers using a special epoxy resin. The ARALL laminates have increased fatigue life and fatigue crack growth properties over monolithic aluminum; the outer aluminum layers provide impact damage and moisture protection that would be a problem for typical fiber composite materials. In addition, increases in strength and lower densities are achieved as compared to monolithic aluminum [38]. Here we analyze the ARALL laminates using the macromechanics elastoplastic formulation discussed earlier.

Figure 20 also shows the description of the analytical model used to represent the stiffness of the ARALL laminates. The aramid epoxy layers are divided into fiber–rich and resin–rich layers. Table 3 contains the properties and statistical distributions for the aluminum, aramid epoxy fiber–rich, and aramid epoxy resin–rich layers. Experimental tension test results [37] are compared with the analytical results in Figure 21. From the figure it is observed that the aramid epoxy behavior is linear and the analytical linear comparison is very good. The 7075–T6(L) aluminum behavior is elastic perfectly–plastic and the analytical model with a yield stress of 78 ksi agrees very well except near the point of first yield. As for the ARALL–1 results (–1 indicates 7075–T6(L) aluminum is used) the analytical model with ideal plasticity for the aluminum layers and linear elastic aramid epoxy layers generally exhibits the same behavior as the experimental results except the 0 degree laminate analytical model underpredicts the stiffness after yield and the 90 degree laminate model overpredicts the stiffness after yield. For the purpose of this example the analytical model is considered acceptable and will be used to study the mean and variance response of an ARALL tension specimen with a hole.

Figure 22a shows the finite element model and dimensions of the tension specimen with a hole problem. The same material properties and material model from the previous discussion are used in this problem. The probabilistic analysis assumed a fully correlated random field for each random function in each layer. Figure 23 contains the mean and standard deviation of the longitudinal ϵ_{yy} strain at the hole edge (point A) for the case where all aramid epoxy layers are aligned at 90 degrees to the load. The figure also shows the breakdown of standard deviations for all the significant random variables. Since the fibers are oriented at 90 degrees to the load and to the strain ϵ_{yy}, then the aluminum properties tend to dominate. It is interesting to note that even though no bending occurs in this problem, the ply thickness of the aluminum layers is dominant after yield. The aluminum yield stress and elastic modulus are also important. Figure 24 contains similar results except now the fibers are aligned with the loading direction. While the aluminum yield stress and ply thickness random variables are still significant, the aramid E_{11} and ply thickness random variables are now equally important. These results illustrate the role the individual random variables play in the total variability of this type of ARALL structure.

Boron/Aluminum Tension Specimen with Hole

A Boron/Aluminum laminate was selected to illustrate the use of the macroscopic orthotropic plasticity formulation. The same problem dimensions (except for thickness) were used as in the last example, however, a different mesh was used that placed gauss points along the x–axis (see Fig. 22b). Rizzi, et al. [28] conducted an experimental and analytical study of this specimen, and provided experimental measurements for the orthotropic elastic constants as well as the a_{ij} values in the yield criterion and the hardening parameters in the isotropic work hardening model. These values are all stated in Table 4 and are used in the present analytical model. It should be noted that the a_{ij} values used in this study differ from those given in the reference by a factor of 2/3 due to a minor difference in the formulations. Figure 25 contains a comparison of the analytical

results from the present study and experimental results from [28] for the longitudinal strain ϵ_{yy} along a radial line (x–axis) 90 degrees to the loading. The agreement is slightly worse than that obtained in [28], but is probably due to the difference in element formulations and the classical incremental plastic stress routine used versus the radial return algorithm used here. Yielding occurs after 1000 lbs, and the agreement worsens as the loading is increased. However, the results are still considered quite good.

Using the random variable statistics stated in Table 4, the first–order second–moment probabilistic method was used to evaluate the mean and variance of the ϵ_{yy} strain response. Once again the probabilistic analysis assumed a fully correlated random field for each random function. Figure 26 shows the analytical mean ϵ_{yy} strain for the 2500 lb and 1000 lb load values with the plus or minus one standard deviation points included. It is obvious that the sensitivity of ϵ_{yy} to the random variables increases both with the load and as the location moves closer to the hole. Figure 27 contains a plot of both the mean and standard deviation of the ϵ_{yy} strain at the location A on the model versus load. The breakdown for each random variable is presented as well. Since only a single layer is used, then the ply thickness could not be considered a variable here. The most significant random variable is the plastic hardening modulus $\bar{H}$, with E_{22} and the yield stress important as well. Note that E_{22} is significant since the fibers are 90 degrees to both the loading direction and to ϵ_{yy}. This example can be extended to include the a_{ij} plastic yield coefficients and the hardening parameter λ as random variables since they are also experimentally measured quantities with uncertainties.

5. Summary

A probabilistic analysis procedure for constitutive behavior of metal matrix composites based on the METCAN program is developed. The procedure can be used to simulate manufacturing nonuniformities and uncertainties in constituent properties to quantify their overall effects on the composite. Studies involving both linear and nonlinear

effects on the thermoelastic and strength properties of two different metal matrix composites were performed. For the case of linear behavior the contributing constituent variations were constrained to the framework of the micromechanics model. Thus, cause and effects for the linear behavior were easy to demonstrate, so that the relative importance of each material variable could be identified. As for the nonlinear effects, since the constituent–based nonlinear material model became active, variations were induced not only by the probabilistic distributions of the constituent properties but also by the distributions of the nonlinear power term parameters such as the melting temperatures and exponents. Thus the nonlinear behavior was really a blend of the variations in the micromechanics model variables and the nonlinear power law variables. It is easy to see how this procedure could be used to aid in material characterization and selection to precede and aid in experimental studies. Much of the results presented have been based on assumed distributions, and thus are intended to be examples illustrating the power of the method.

A formulation based on a macromechanics orthotropic elastoplasticity theory is also presented. A nonlinear probabilistic finite element analysis procedure including elastoplastic constitutive behavior is developed. The first–order second–moment method for probabilistic finite element analysis was combined with a continuum shell element which includes the effects of shear deformation. Both ARALL and Boron/Aluminum plasticity problems were investigated, and the variability of these composites was quantified for a tension specimen with a hole.

References

1. CHAMIS, C. C. and HOPKINS, D. A. – A Unique Set of Micromechanics Equations for High Temperature Metal Matrix Composites, NASA Technical Memorandum 87154, 1985.

2. CHAMIS, C. C. and HOPKINS, D. A. – Thermoviscoplastic Nonlinear Constitutive Relationships for Structural Analysis of High Temperature Metal Matrix Composites, NASA Technical Memorandum 87291, 1985.

3. HOPKINS, D. A. – Nonlinear Analysis for High–Temperature Multilayered Fiber Composite Structures, NASA Technical Memorandum 83754, 1984.

4. STOCK, T. A. – *Probabilistic Fiber Composite Micromechanics*, Masters Thesis, Civil Engineering, Cleveland State University, 1987.

5. DVORAK, G. J., RAO, M. S. M. and TARN, J. Q. – Yielding in Unidirectional Composites Under External Loads and Temperature Changes, *J. Composite Materials*, Vol. 7, 1973, p. 194.

6. DVORAK, G. J., RAO, M. S. M. and TARN, J. Q. – Generalized Initial Yield Surfaces for Unidirectional Composites, *J. Appl. Mech.*, Vol. 41, 1974, p. 249.

7. DVORAK, G. J., and RAO, M. S. M. – Axisymmetric Plasticity Theory of Fibrous Composites, *Int. J. Engng. Sci.*, Vol. 14, 1976, p. 361.

8. DVORAK, G. J., and RAO, M. S. M. – Thermal Stress in Heat–Treated Fibrous Composites, *J. Appl. Mech.*, Vol. 43, 1976, p. 619.

9. DVORAK, G. J., and BAHEI–EL–DIN, Y. A. – Elastic–Plastic Behavior of Fibrous Composites, *J. Mech. Phys. Solids*, Vol. 27, 1979, p. 51.

10. BAHEI–EL–DIN, Y. A. and DVORAK, G. J. – Plastic Yielding at a Circular Hole in a Laminated FP–Al Plate, *Modern Development in Composite Materials and Structures*, Vinson, J. R., ed., The American Society of Mechanical Engineers, 1979, p. 123.

11. BAHEI–EL–DIN, Y. A., DVORAK, G. J. and UTKU, S. – Finite Element Analysis of Elastic–Plastic Fibrous Composite Structures, *Computers and Structures*, Vol. 13, 1981, p. 321.

12. BAHEI–EL–DIN, Y. A. and DVORAK, G. J. – Plasticity Analysis of Laminated Composite Plates, *J. Appl. Mech.*, Vol. 49, 1982, p. 740.

13. TEPLY, J. L. – Periodic Hexagonal Array Models for Plasticity Analysis of Composite Materials, University of Utah, Ph.D. Dissertation, 1984.

14. TEPLY, J. L., and DVORAK, G. J. – Bounds on Overall Instantaneous Properties of Elastic–Plastic Composites, *J. Mech. Phys. Solids*, Vol. 36, 1988, p. 29.

15. ABOUDI, J. – A Continuum Theory for Fiber–Reinforced Elastic–Viscoplastic Composites, *Int. J. Engng. Sci.*, Vol. 20, 1982, p. 605.

16. ABOUDI, J. – Effective Moduli of Short–Fiber Composites, *Int. J. Solids and Structures*, Vol. 19, 1983, p. 693.

17. ABOUDI, J. – Elastoplasticity Theory for Composite Materials, *Solid Mech. Arch.*, Vol. 11, 1986, p. 141.

18. ABOUDI, J. – Damage in Composites: Modeling of Imperfect Bonding, *Composite Sci. Tech.*, Vol. 28, 1987, p. 103.

19. ABOUDI, J. – Closed Form Constitutive Equations for Metal Matrix Composites, *Int. J. Engng. Sci.*, Vol. 25, 1987, p. 1229.

20. ABOUDI, J. – Constitutive Equations for Elastoplastic Composites with Imperfect Bonding, *Int. J. Plasticity*, June, 1988.

21. ACHENBACK, J. D., *A Theory of Elasticity with Microstructures for Directionally Reinforced Composites*, Springer–Verlag, New York, 1975.

22. SUN, C. T., ACHENBACH, J. D. and HERMANN, G. – Continuum Theory for a Laminated Medium, *J. Appl. Mech.*, Vol. 35, 1968, p. 467.

23. TEPLY, J. L. and REDDY, J. N. – A Unified Formulation of Micromechanics Models of Fiber–Reinforced Composites, in *Inelastic Deformation of Composite Materials*, G. J. Dvorak (eds.), Springer–Verlag, New York, 1990, pp. 341–370.

24. ARENBURG, R. T. and REDDY, J. N. – Elastoplastic Analysis of Metal Matrix Composite Structures, Technical Report No. CCMS–89–02, 1989, Virginia Tech Center for Composite Materials and Structures, Blacksburg, Virginia.

25. ARENBURG, R. T. and REDDY, J. N. – Analysis of Metal–Matrix Composite Structures, *Computers and Structures*, Vol. 40, 1991, p. 1357.

26. HILL, R. – A Theory of the Yielding and Plastic Flow of Anisotropic Metals, *Proc. Roy. Soc.*, Vol. 193, No. 1033, 1948, p. 189.

27. SUN, C. T. and CHEN, J. K. – Effect of Plasticity on Free Edge Stresses in Boron–Aluminum Composite Laminates, *J. of Composite Materials*, Vol. 21, 1987, p. 969.

28. RIZZI, S. A., LEEWOOD, A. R., DOYLE, J. F., and SUN, C. T. – Elastic–Plastic Analysis of Boron/Aluminum Composite Under Constrained Plasticity Conditions, *J. of Composite Materials*, Vol. 21, 1987, p. 734.

29. CHAO, W. C. and REDDY, J. N. – Analysis of Laminated Composite Shells Using a Degenerated 3–D Element, *Int. J. Numerical Methods in Engineering*, Vol. 20, 1984, p. 1991.

30. LIAO, C. L. and REDDY, J. N. – A Continuum–Based Stiffened Composite Shell Element for Geometrically Nonlinear Analysis, *AIAA Journal*, Vol. 27, No. 1, 1989, p. 95.

31. SIMO, J. C. and HUGHES, T. J. R., *Elastoplasticity and Viscoplasticity Computational Aspects*, Draft of unpublished book, 1988.

32. SIMO, J. C. and TAYLOR, R. L. – A Return Mapping Algorithm for Plane Stress Elastoplasticity, *Int. J. for Numerical Methods in Engineering*, Vol. 22, No. 3, 1986, p. 649.

33. LIU, W. K., BELYTSCHKO, T., and MANI, A. – Random Field Finite Elements, *Int. J. for Numerical Methods in Engineering*, Vol. 23, 1986, p. 1831.

34. LIU, W. K., BELYTSCHKO, T. and MANI, A. – Probabilistic Finite Elements for Nonlinear Structural Dynamics, *Computer Methods in Applied Mechanics and Engineering*, Vol. 56, 1986, p. 61.

35. NAKAGIRI, S., TAKABATAKE, H. and TANI, S. – Uncertain Eigenvalue Analysis of Composite Laminated Plates by the Stochastic Finite Element Method, *ASME J. of Engineering for Industry*, Vol. 109, No. 1, February 1987, p. 9.

36. BECKER, W., *Mechanical Response of Unidirectional Boron/Aluminum Under Combined Loading*, M.S. Thesis, Virginia Polytechnic Institute and State University, Blacksburg, Virginia, 1987.

37. BUCCI, R. J. and MUELLER, L. N. – ARALL Laminate Performance Characteristics, presented at ARALL Laminates Technical Conference, Seven Springs Resort, Champion, PA, 1987.

38. ENGELSTAD, S. P. and REDDY, J. N. – Nonlinear Probabilistic Finite Element Models of Laminated Composite Shells, Technical Report No. CCMS–91–02, January 1991, Virginia Tech Center for Composite Materials and Structures, Blacksburg, Virginia.

TABLE 1

Input Statistical Parameters for Graphite Copper

Input		Case 1	Case 2
Normally Distributed Variables	μ	σ	σ
Ply Angle (degrees)	0.0	5.0	10.0
Fiber Volume Ratio (FVR)	0.5	0.1	0.2
E_{f11}(GPa)	723.9	36.2	72.4
E_{f22}(GPa)	6.2	0.3	0.6
G_{f12}(GPa)	7.6	0.4	0.8
G_{f23}(GPa)	4.8	0.24	0.48
E_m(GPa)	122.0	6.1	12.2
E_d(GPa)	275.8	13.8	27.6
Interphase % of fiber diameter	0.10	0.005	0.01
Weibull Distributed Variables	β	λ	λ
S_{f11t}(MPa)	2240.8	20	10
S_{f11c}(MPa)	1378.9	20	10
S_{f22t}(MPa)	172.4	20	10
S_{f22c}(MPa)	172.4	20	10
S_{f12s}(MPa)	172.4	20	10
S_{f23s}(MPa)	86.2	20	10
S_m(MPa)	220.6	20	10
S_{ms}(MPa)	131.0	20	10
S_d(MPa)	103.4	20	10
S_{ds}(MPa)	68.9	20	10
Gamma Distributed Variables	β	λ	λ
Void Volume Ratio (VVR)	0.33	3.0	5.0

TABLE 2

Input Statistical Parameters for SCS–6 TI15

Normally Distributed Variables	μ	σ
Ply Angle (degrees)	0.0	0.5
E_{f11}(GPa)	349.6	17.5
E_{f22}(GPa)	349.6	17.5
G_{f12}(GPa)	146.9	7.3
G_{f23}(GPa)	146.9	7.3
E_m(GPa)	84.8	4.2
E_d(GPa)	275.8	13.8
T_{Mf}(°K)	2755.4	107.2
T_{Mm}(°K)	1255.4	32.2
T_{Md}(°K)	2199.9	79.4
Fiber Exponents	0.25	0.0125
Matrix Exponents	0.50	0.025
Interphase Exponents	0.50	0.025
Interphase % of fiber diameter	0.10	0.005
α_{f11}	0.12E–5	0.60E–7
α_{f22}	0.12E–5	0.60E–7
α_m	0.45E–5	0.225E–6
α_d	0.5E–5	0.25E–6
Weibull Distributed Variables	β	λ
S_{f11t}(MPa)	3350.9	20
S_{f11c}(MPa)	3350.9	20
S_{f22t}(MPa)	3350.9	20
S_{f22c}(MPa)	3350.9	20
S_{f12s}(MPa)	1675.4	20
S_{f23s}(MPa)	1675.4	20
S_m(MPa)	896.3	20
S_{ms}(MPa)	627.4	20
S_d(MPa)	103.4	20
S_{ds}(MPa)	68.9	20
N_{MF}(cycles)	1.0E6	20
Gamma Distributed Variables	β	λ
Void Volume Ratio (VVR)	0.33	3.0

TABLE 3

Material Properties and Statistics for ARALL–1 Laminate Constituents

Random Variable	Mean	Standard Deviation	Coefficient of Variation
Aluminum (7075–T6L)			
E	10.4×10^{6}	5.2×10^{5}	0.05
ν	0.3	1.5×10^{-2}	0.05
σ_Y^*	7.8×10^{4}	3.9×10^{3}	0.05
δ^*	1.2×10^{-2}	6.0×10^{-4}	0.05
Aramid Epoxy fiber–rich layers			
E_{11}	12.549×10^{6}	6.2745×10^{5}	0.05
E_{22}	0.76525×10^{6}	3.82625×10^{4}	0.05
G_{12}	0.28955×10^{6}	1.44775×10^{4}	0.05
ν_{12}	0.3458	1.729×10^{-2}	0.05
G_{13}	0.28955×10^{6}	1.44775×10^{4}	0.05
θ^*	0°,90°	2°	–
δ^*	5.6×10^{-3}	2.8×10^{-4}	0.05
Aramid Epoxy resin–rich layers			
E_{11}	2.1972×10^{6}	1.0986×10^{5}	0.05
E_{22}	0.48219×10^{6}	2.41095×10^{4}	0.05
G_{12}	0.15717×10^{6}	7.8585×10^{3}	0.05
ν_{12}	0.3749	1.8745×10^{-2}	0.05
G_{13}	0.15717×10^{6}	7.8585×10^{3}	0.05
G_{23}	0.15576×10^{6}	7.7880×10^{3}	0.05
θ^*	0°,90°	2°	–
δ^*	1.416×10^{-3}	7.08×10^{-5}	0.05

*σ_Y indicates yield stress, θ indicates fiber orientation angle, and δ indicates ply thickness.
Units are in psi and inches where appropriate.

TABLE 4

Material Properties and Statistics for Boron/Aluminum Laminate

Random Variable	Mean	Standard Deviation	Coefficient of Variation
E_{11}	29.4×10^{6}	1.47×10^{6}	0.05
E_{22}	19.1×10^{6}	9.55×10^{5}	0.05
G_{12}	7.49×10^{6}	3.745×10^{5}	0.05
ν_{12}	0.169	8.45×10^{-3}	0.05
G_{13}	7.49×10^{6}	3.745×10^{5}	0.05
G_{23}	7.49×10^{6}	3.745×10^{5}	0.05
σ_Y^*	13.5×10^{3}	6.75×10^{2}	0.05
$\bar{H}^*$	60.0×10^{3}	3.0×10^{3}	0.05
θ^*	0°	2.0°	—
δ^*	7.95×10^{-2}	—	0.05

*σ_Y indicates yield stress, $\bar{H}$ indicates hardening modulus, θ indicates ply orientation angle, and δ indicates ply thickness.
The values of the a_{ij} constants in the yield criterion are:

$$\frac{3}{2}a_{11} = 0.001 \ , \ \frac{3}{2}a_{22} = 1.0 \ , \ \frac{3}{2}a_{12} = -0.01$$

$$\frac{3}{2}a_{44} = \frac{3}{2}a_{55} = \frac{3}{2}a_{66} = 1.9$$

The hardening model used was $Y(\alpha) = \bar{H}[\alpha + [\frac{\sigma_{Y_1}}{\bar{H}}]^{\lambda}]^{1/\lambda}$

$$\lambda = 5.8$$

Units are in psi and inches where appropriate.

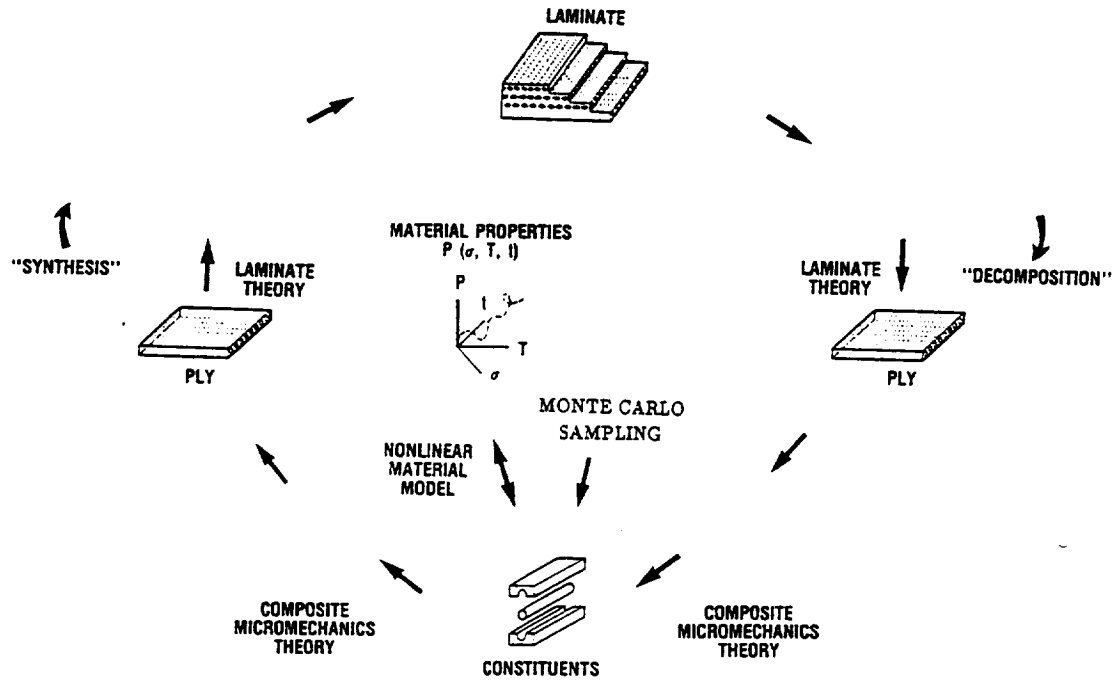

Figure 1. Probabilistic integrated multi-scale metal matrix composite analysis.

$$\frac{P}{P_0} = \left[\frac{T_F - T}{T_F - T_0}\right]^n \left[\frac{S_F - \sigma}{S_F - \sigma_0}\right]^m \left[\frac{\dot{S}_F - \dot{\sigma}_0}{\dot{S}_F - \dot{\sigma}}\right]^\ell \left[\frac{\dot{T}_F - \dot{T}}{\dot{T}_F - \dot{T}_0}\right]^k \left[\frac{R_F - R}{R_F - R_0}\right]^p \cdots$$

$$\cdots \left[\frac{N_{MF} - N_M}{N_{MF} - N_{MO}}\right]^q \left[\frac{N_{TF} - N_T}{N_{TF} - N_{TO}}\right]^r \left[\frac{t_F - t}{t_F - t_0}\right]^s \cdots$$

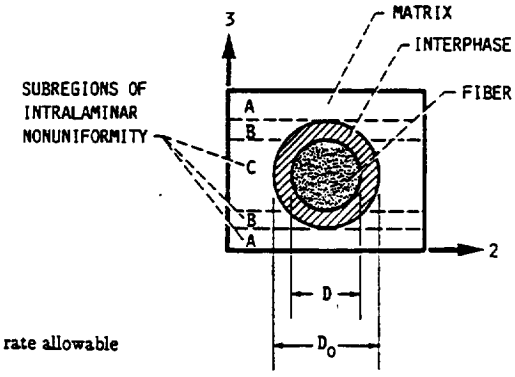

SYMBOLS

P	Property	$\dot{S}$	Stress rate allowable
S	Strengths	σ	Stress
T_M	Melting temperature	$\dot{\sigma}$	Stress rate
T_o	Room temperature	t	Time
T	Current or use temperature	subscripts o,F	Reference and final values
N_{TF}	Thermal cyclic limit		
N_{MF}	Mechanical cyclic limit		

Figure 2. Multi-factor constituent material model and micromechanics subcell.

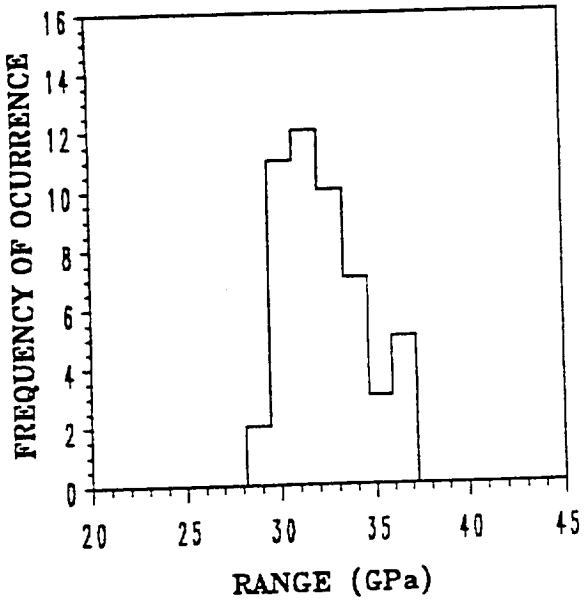

(a) Case 1 histogram (narrow range)

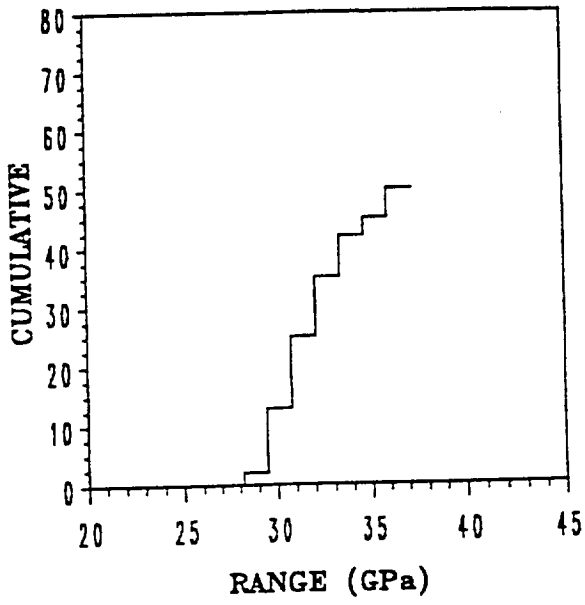

(b) Case 1 cumulative distribution

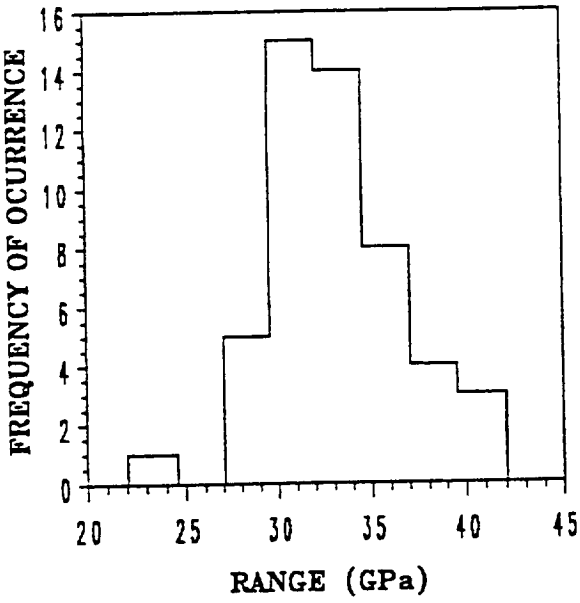

(c) Case 2 histogram (wide range)

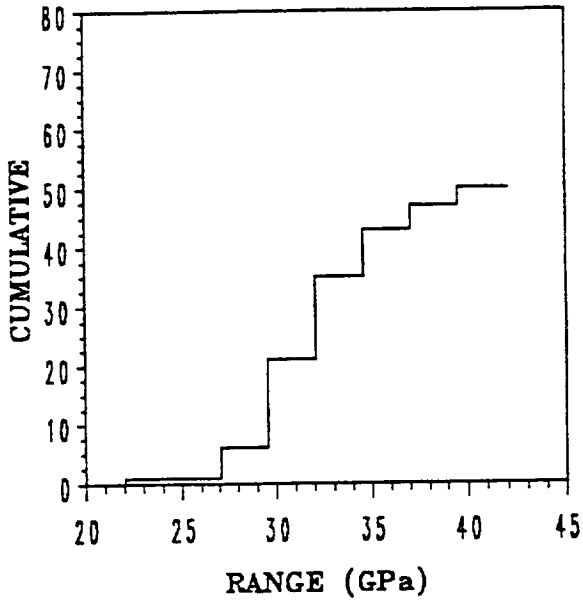

(d) Case 2 cumulative distribution

Figure 3. Histograms and cumulative distribution curves for in-plane shear modulus $G_{\ell 12}$

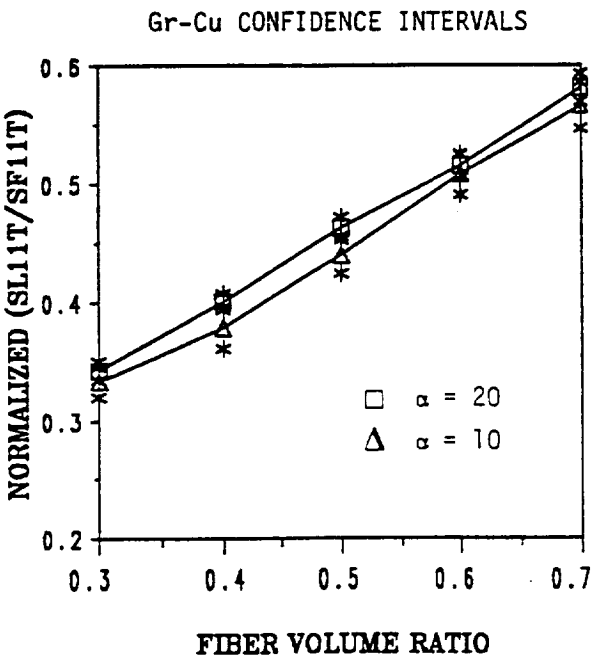

Figure 4. Longitudinal tensile strength with perturbed shape parameter of fiber strength.

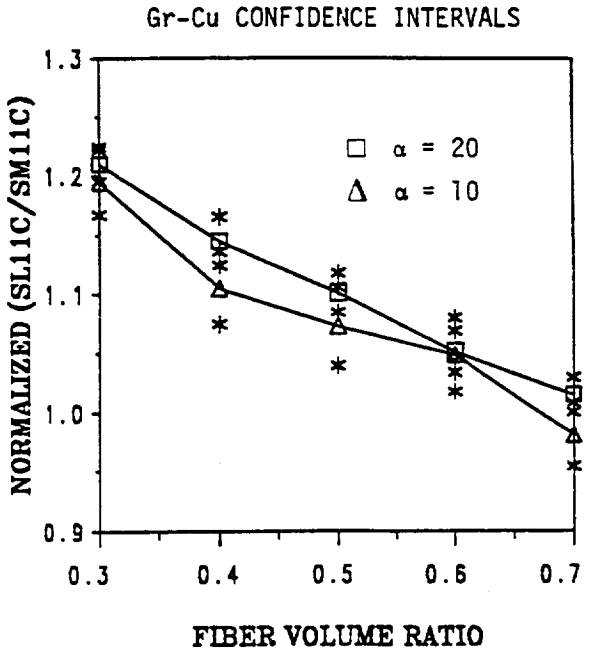

Figure 5. Longitudinal compressive strength with perturbed shape parameter of matrix strength.

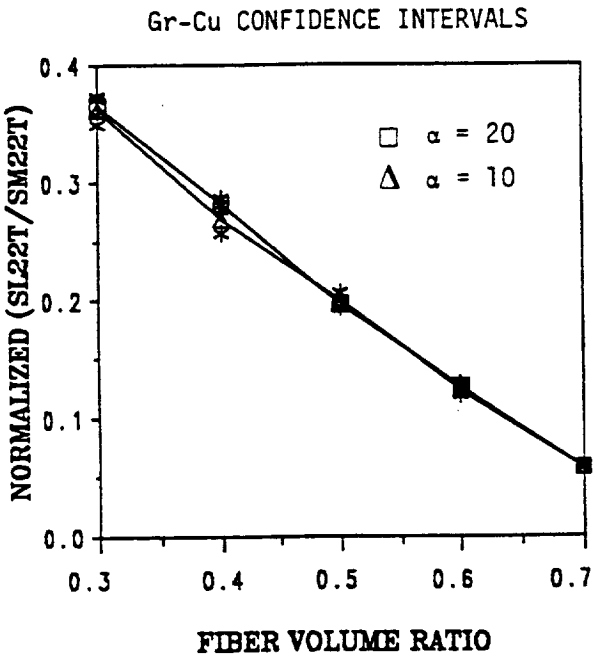

Figure 6. Transverse tensile strength with perturbed shape parameter of matrix strength.

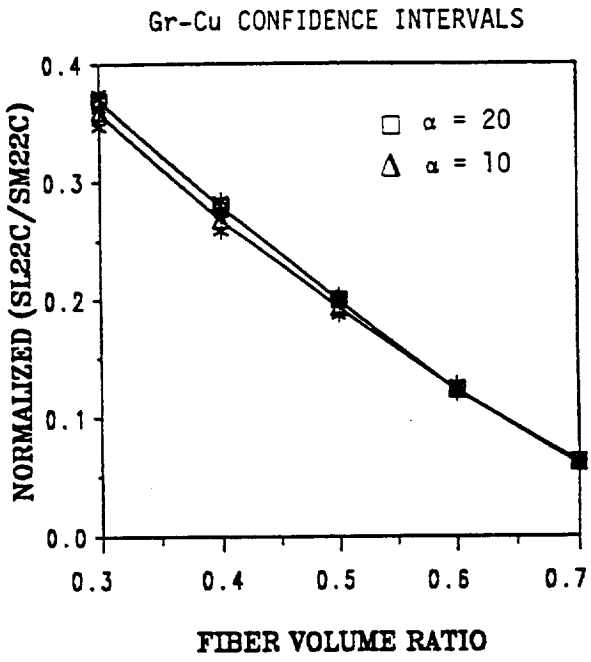

Figure 7. Transverse compressive strength with perturbed shape parameter of matrix strength.

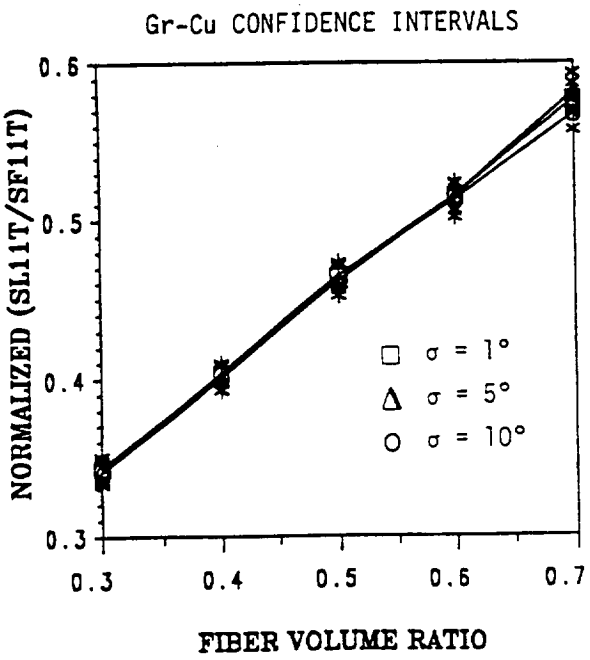

Figure 8. Longitudinal tensile strength with perturbed COV of fiber angle.

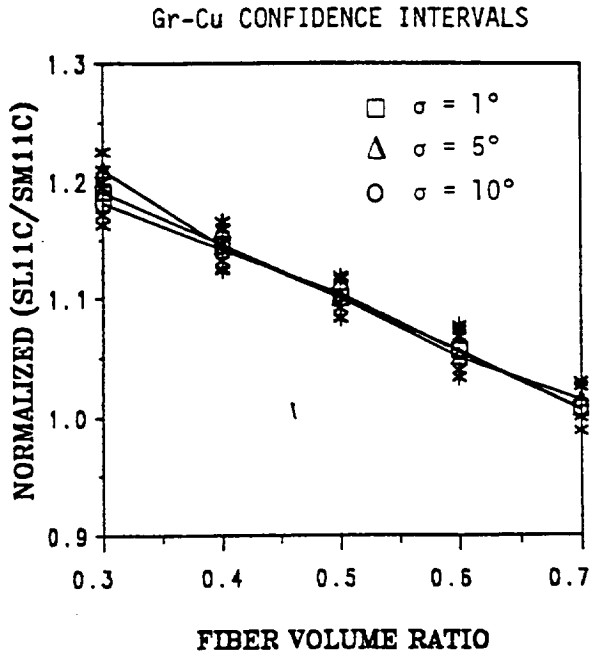

Figure 9. Longitudinal compressive strength with perturbed COV of fiber angle.

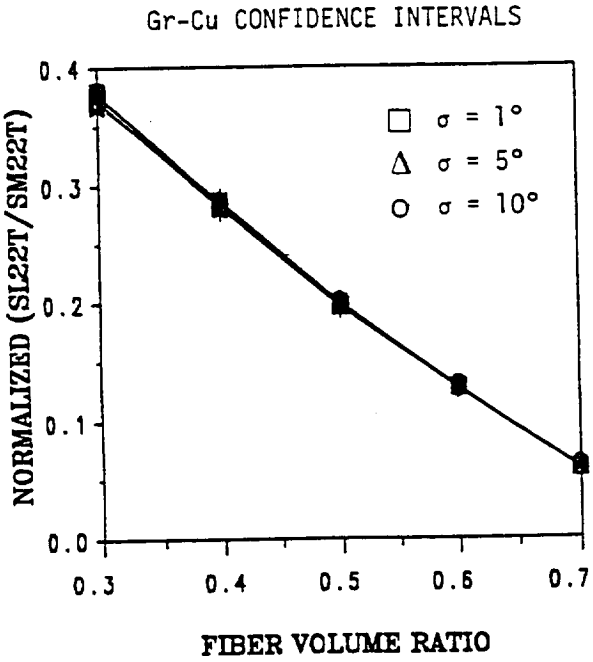

Figure 10. Transverse tensile strength with perturbed COV of fiber angle.

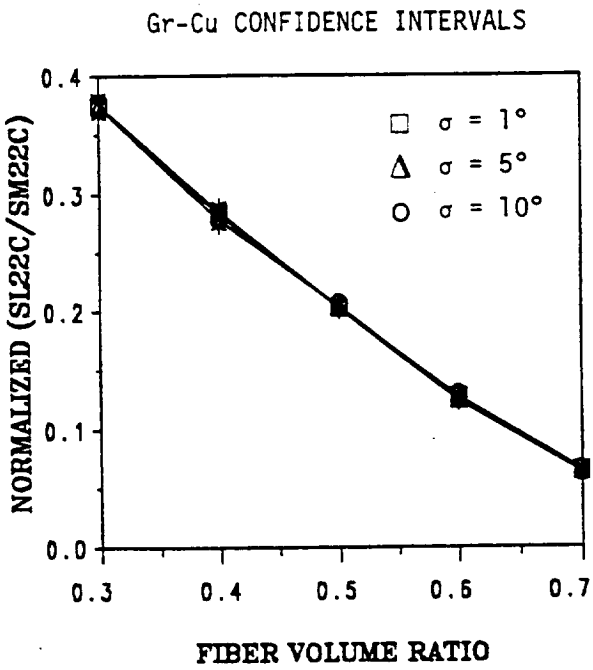

Figure 11. Transverse compressive strength with perturbed COV of fiber angle.

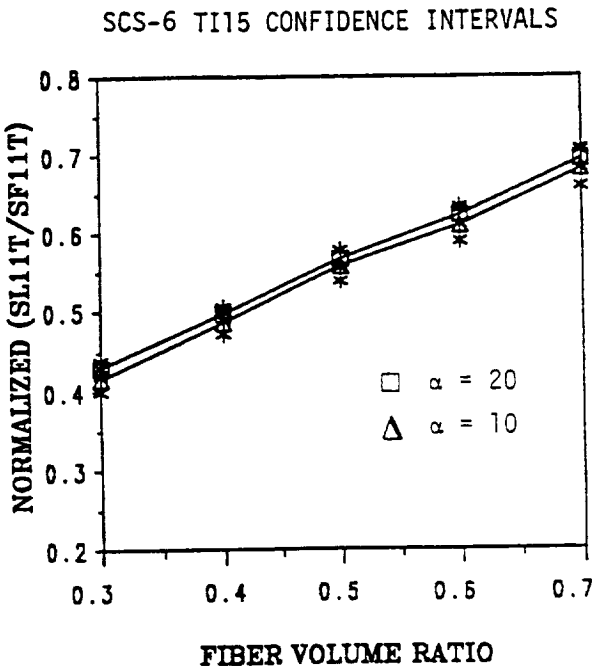

Figure 12. Longitudinal tensile strength with perturbed shape parameter of fiber strength; power law inactive.

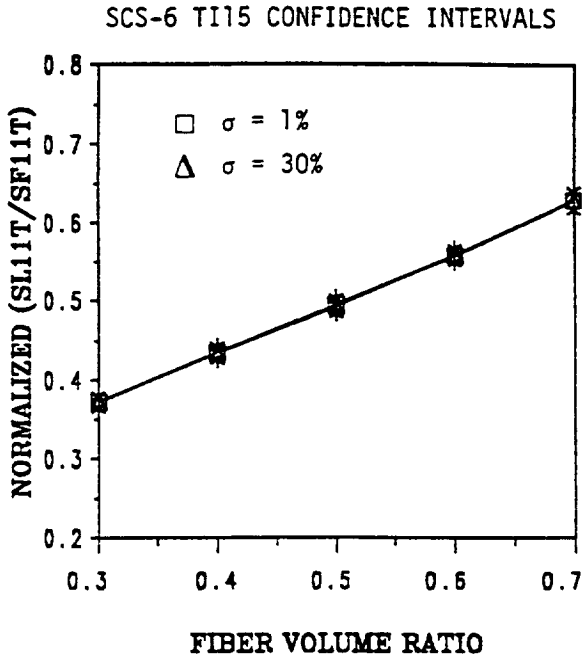

Figure 13. Longitudinal tensile strength with perturbed COV of fiber strength temperature exponent n; temperature power term active.

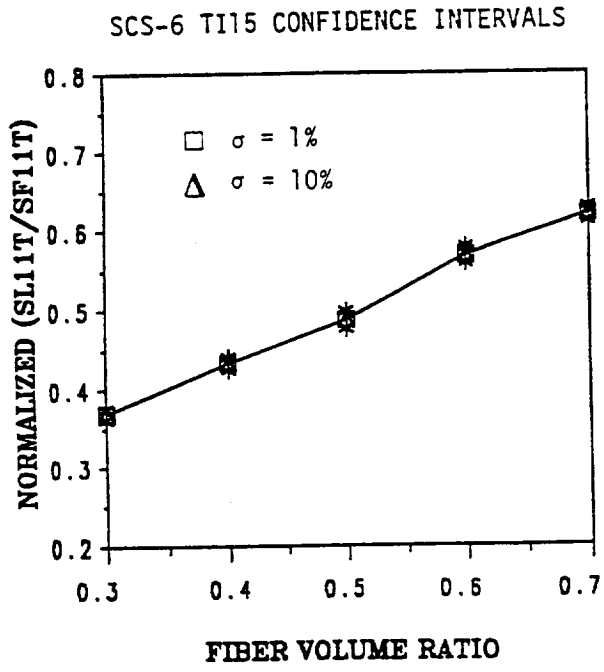

Figure 14. Longitudinal tensile strength with perturbed COV of fiber melting temperature; temperature power term active.

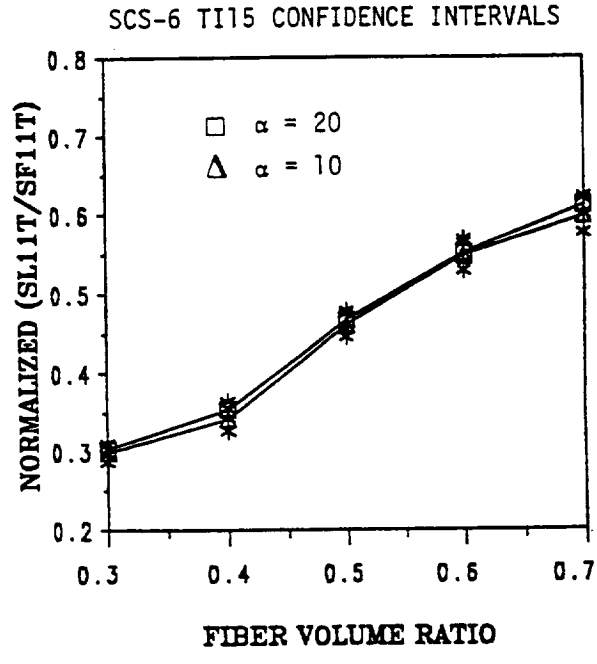

Figure 15. Longitudinal tensile strength with perturbed shape parameter of fiber strength; stress power term active.

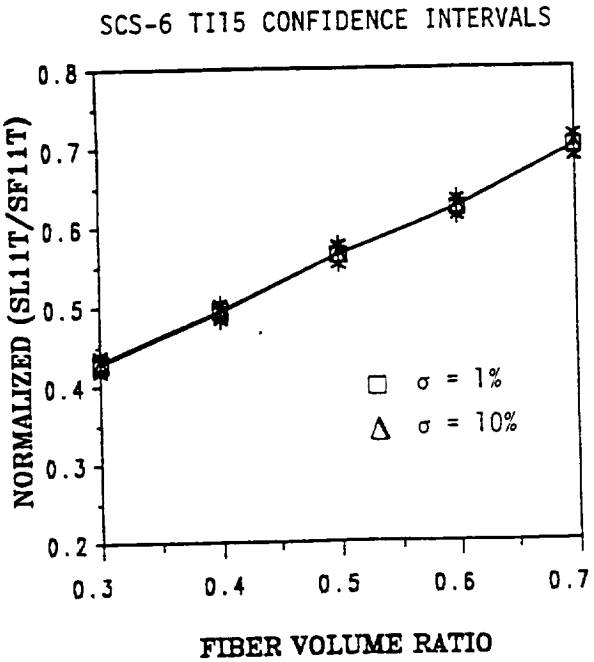

Figure 16. Longitudinal tensile strength with perturbed COV of matrix modulus; power law inactive.

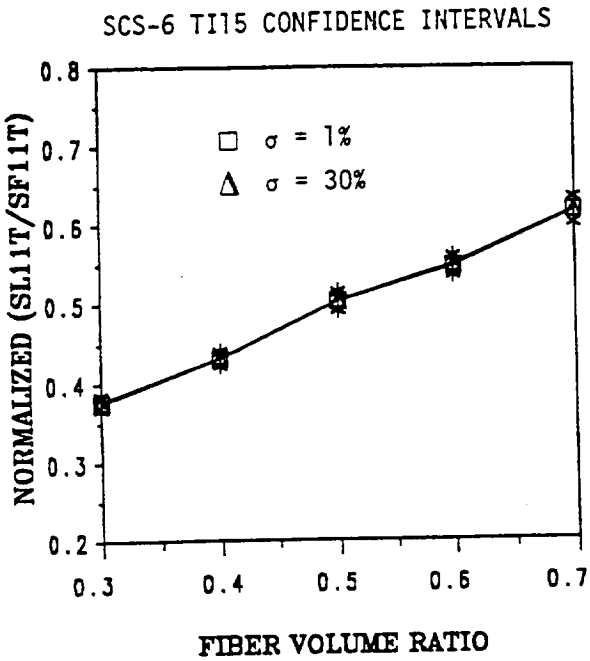

Figure 17. Longitudinal tensile strength with perturbed COV of matrix modulus temperature exponent n; temperature power term active.

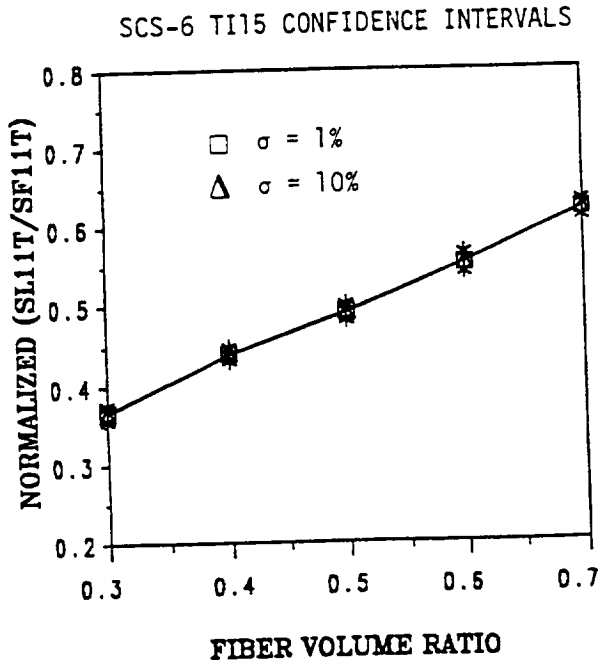

Figure 18. Longitudinal tensile strength with perturbed COV of matrix melting temperature; temperature power term active.

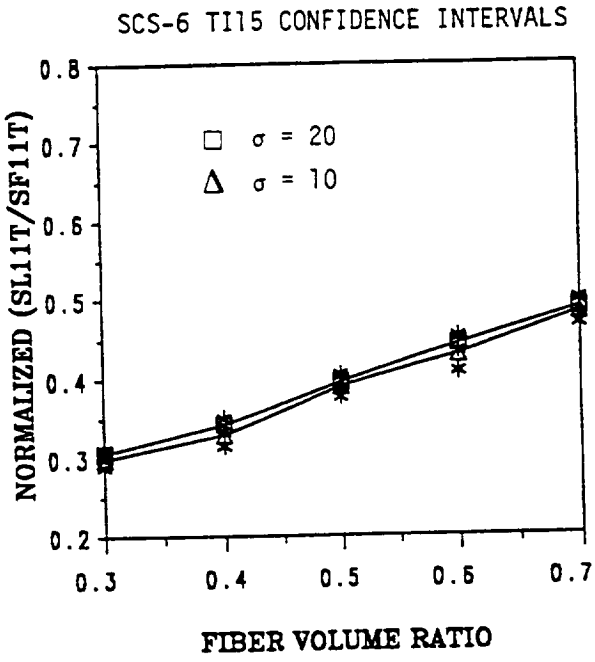

Figure 19. Longitudinal tensile strength with perturbed shape parameter of mechanical strength; mechanical cycle power term active.

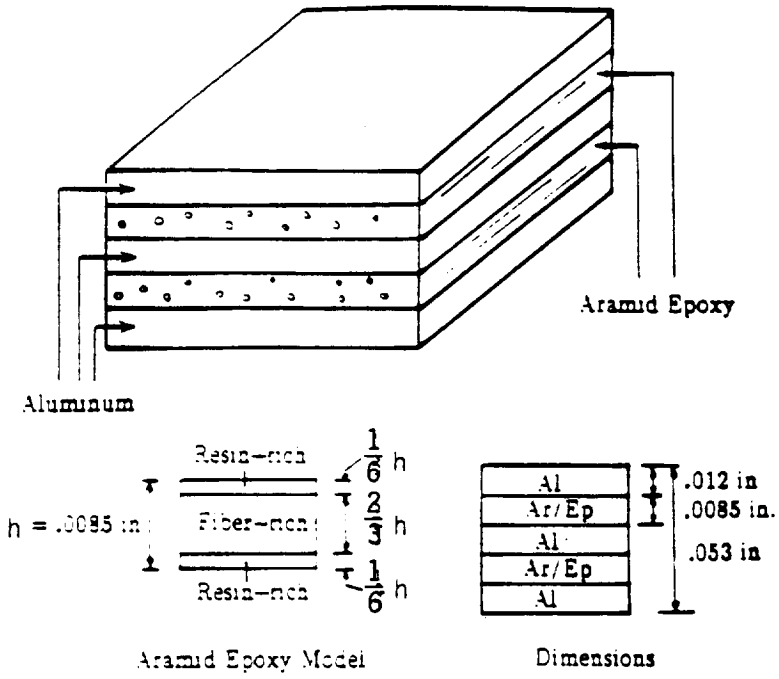

Figure 20. ARALL laminate layup and geometry.

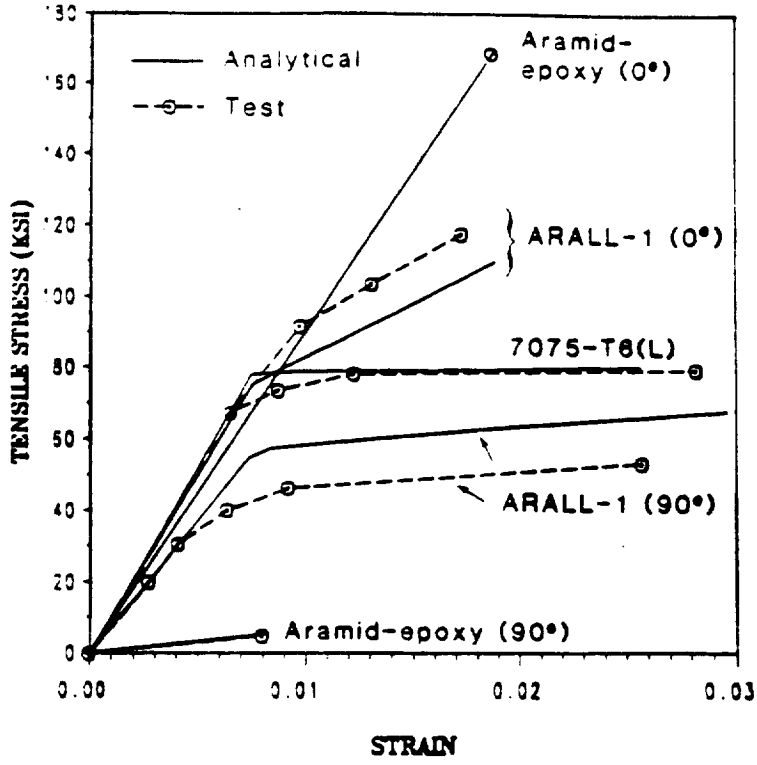

Figure 21.ARALL tesnsion test experimental and analytical comparisons.

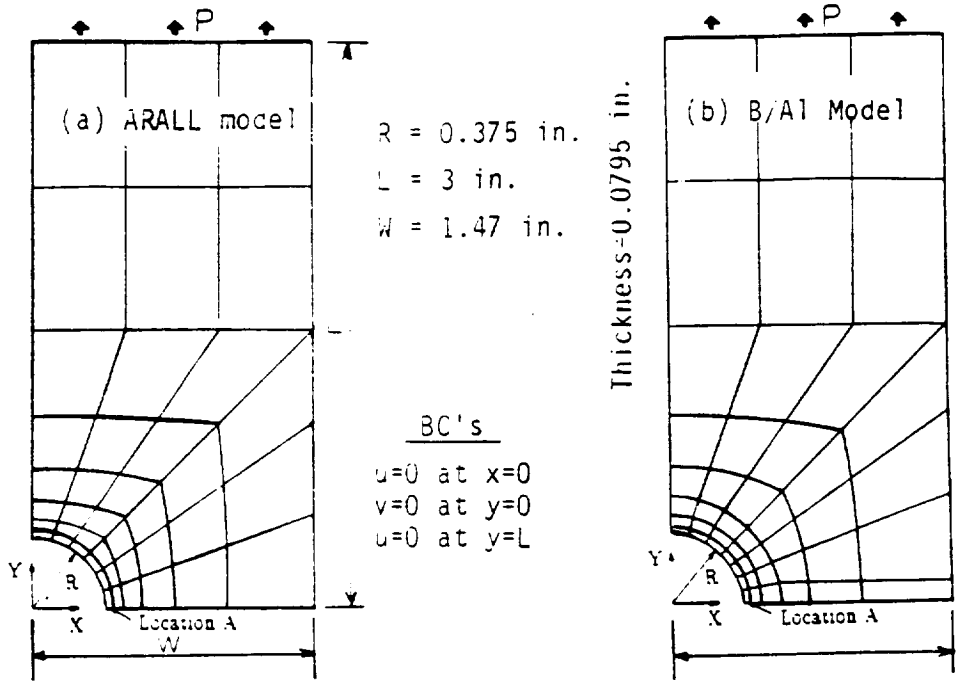

Figure 22. Finite element mesh, loading and boundary conditions of a tension specimen with a hole.

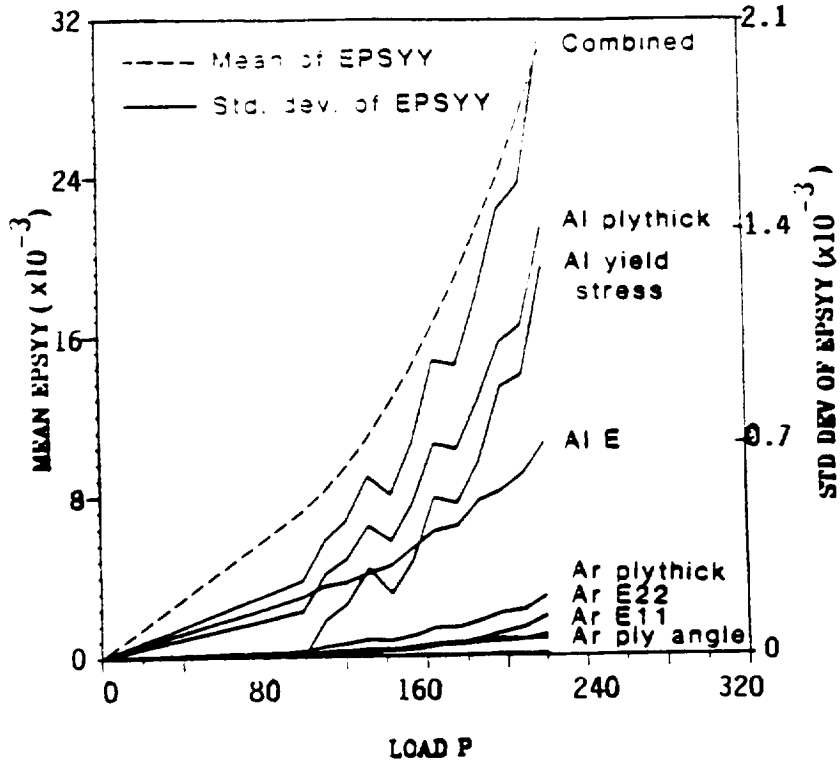

Figure 23. Mean and standard deviation of normal strain at the hole edge (point A) versus load for the case where the fibers are at 90° to the load.

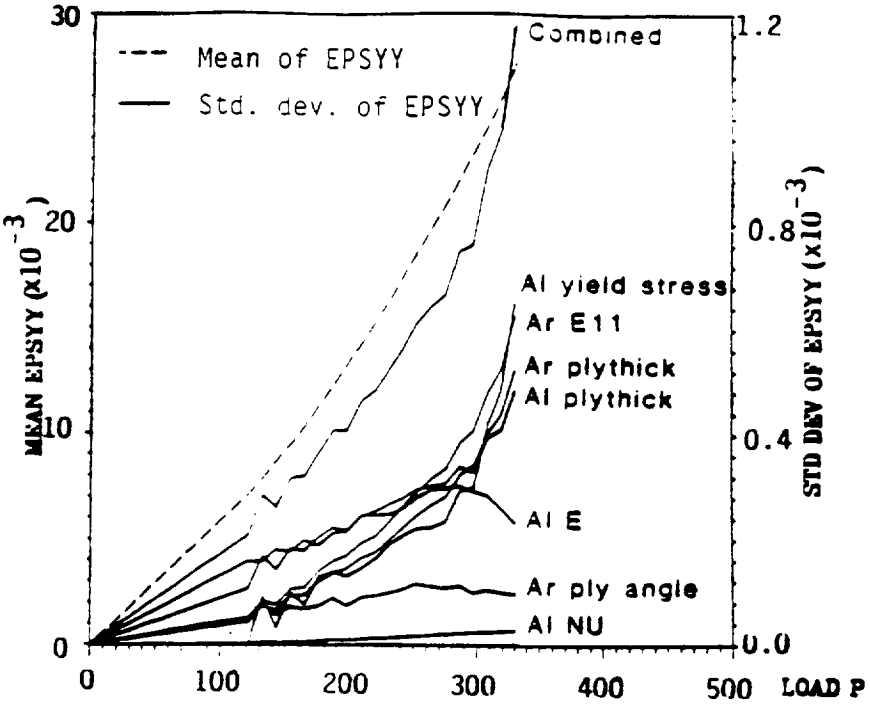

Figure 24. Mean and standard deviation of normal strain at the hole edge (point A) versus load for the case where fibers are aligned with the load.

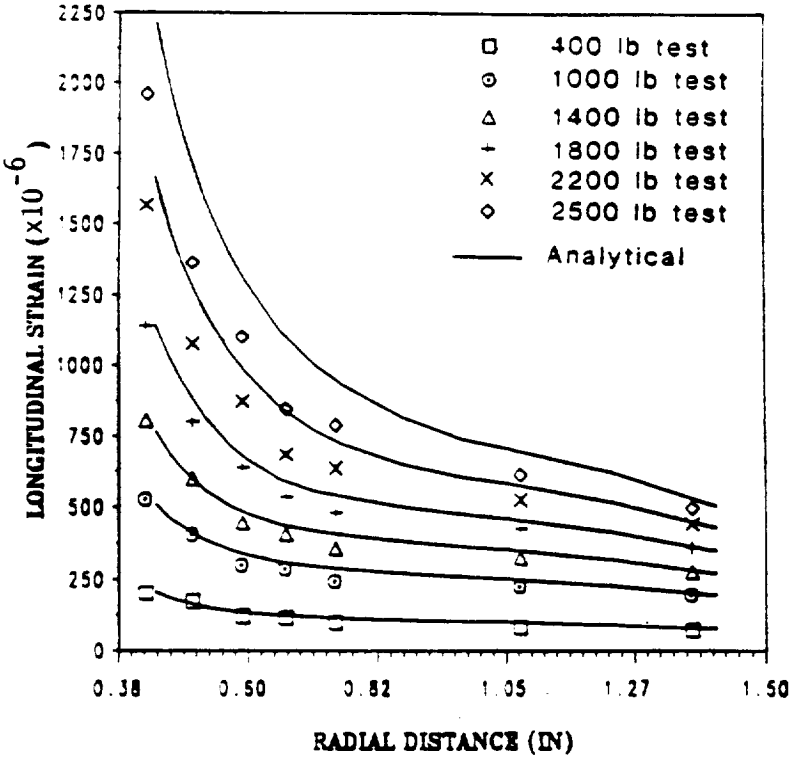

Figure 25. Analytical and experimental comparison of the longitudinal strain along a line 90° to the loading for the Boron/Aluminum laminate.

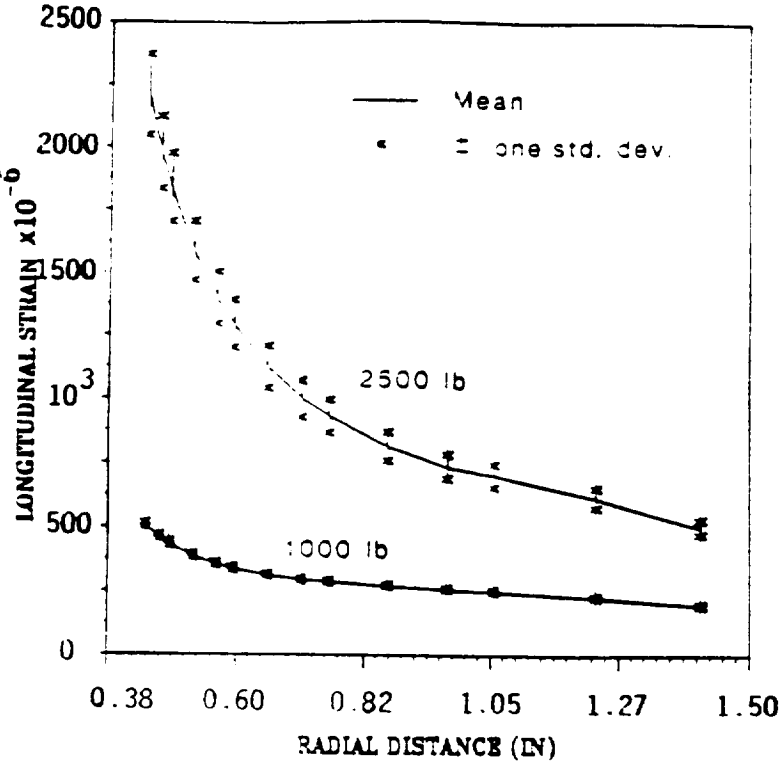

Figure 26. Distribution of the longitudinal strain along a line 90° to the loading for the Boron/Al laminate tension specimen with hole.

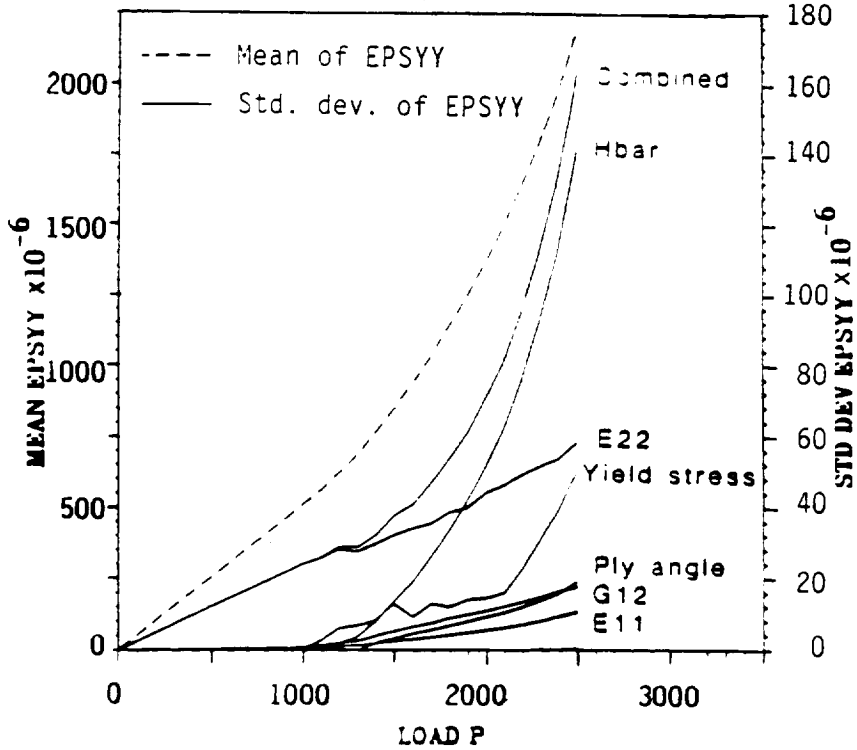

Figure 27. Mean and standard deviation of normal strain at the hole edge (point A) versus load for the Boron/Aluminum tension specimen with hole.

REPORT DOCUMENTATION PAGE

Form Approved
OMB No. 0704-0188

1. AGENCY USE ONLY (*Leave blank*)	2. REPORT DATE	3. REPORT TYPE AND DATES COVERED
	September 1993	Final Contractor Report

4. TITLE AND SUBTITLE

Probabilistic Micromechanics for High-Temperature Composites

5. FUNDING NUMBERS

WU-510-01-50
C-NAG3-933

6. AUTHOR(S)

J.N. Reddy

7. PERFORMING ORGANIZATION NAME(S) AND ADDRESS(ES)

Virginia Polytechnic Institute and State University
Department of Engineering Science and Mechanics
Blacksburg, Virginia 24061

8. PERFORMING ORGANIZATION REPORT NUMBER

E-8113

9. SPONSORING/MONITORING AGENCY NAME(S) AND ADDRESS(ES)

National Aeronautics and Space Administration
Lewis Research Center
Cleveland, Ohio 44135-3191

10. SPONSORING/MONITORING AGENCY REPORT NUMBER

NASA CR-191150

11. SUPPLEMENTARY NOTES

Project Manager, D.A. Hopkins, Structures Division, (216) 433-3260.

12a. DISTRIBUTION/AVAILABILITY STATEMENT

Unclassified - Unlimited
Subject Category 39

12b. DISTRIBUTION CODE

13. ABSTRACT (*Maximum 200 words*)

The three-year program of research had the following technical objectives: the development of probabilistic methods for micromechanics-based constitutive and failure models, application of the probabilistic methodology in the evaluation of various composite materials and simulation of expected uncertainties in unidirectional fiber composite properties, and influence of the uncertainties in composite properties on the structural response. The first year of research was devoted to the development of probabilistic methodology for micromechanics models. The second year of research focused on the evaluation of the Chamis-Hopkins constitutive model and Aboudi constitutive model using the methodology developed in the first year of research. The third year of research was devoted to the development of probabilistic finite element analysis procedures for laminated composite plate and shell structures.

14. SUBJECT TERMS	15. NUMBER OF PAGES
Composites; Micromechanics; Finite element method; Plate; Shell; Probabilistic analysis	45
	16. PRICE CODE A03

17. SECURITY CLASSIFICATION OF REPORT	18. SECURITY CLASSIFICATION OF THIS PAGE	19. SECURITY CLASSIFICATION OF ABSTRACT	20. LIMITATION OF ABSTRACT
Unclassified	Unclassified	Unclassified	